CHAPTER 1

Low-temperature Chemistry in Uniform Supersonic Flows

M. FOURNIER[a], S. D. LE PICARD[b] AND I. R. SIMS*[b]

[a]Combustion Research Facility, Sandia National Laboratories, Livermore, CA 94550, USA; [b]Institut de Physique de Rennes, UMR CNRS-UR1 6251, Université de Rennes 1, 263 Avenue du Général Leclerc, 35042 Rennes Cedex, France
*E-mail: ian.sims@univ-rennes1.fr

1.1 Introduction

Enormous progress has been achieved over the past several decades in the determination of gas-phase rate constants for elementary reactions, especially at high temperatures relevant to combustion ($T > ca.\ 500$ K). At sub-ambient temperatures progress has been slower, despite strong interest in reaction kinetics data from the atmospheric and astrochemical communities, as well as for fundamental tests of rate constant theory. This is due in no small measure to the considerable experimental difficulties associated with low-temperature kinetics measurements, but perhaps also to the commonly-held belief that the temperature-dependent rate constants $k(T)$ of chemical reactions are almost universally described by the well-known Arrhenius equation

$$k(T) = A\exp(-E_{\mathrm{act}}/RT), \tag{1.1}$$

where A is the Arrhenius pre-exponential factor, R is the universal gas constant, T the temperature, and E_{act} is the activation energy, or at least by the

Theoretical and Computational Chemistry Series No. 11
Cold Chemistry: Molecular Scattering and Reactivity Near Absolute Zero
Edited by Olivier Dulieu and Andreas Osterwalder

Published by the Royal Society of Chemistry, www.rsc.org

modified form of this equation in which additional temperature dependence is allowed for in the pre-exponential term

$$k(T) = A'T^{\mathrm{m}}\exp(-E'_{\mathrm{act}}/RT). \tag{1.2}$$

The origin of and justification for these equations, which, though bearing Arrhenius' name, owe more to the work of Van't Hoff, have been discussed recently by Ian W. M. Smith.[1] The temperature dependence of the rate constant for a reaction obeying the Arrhenius equation may be represented by the much-used Arrhenius plot of the log of $k(T)$ as a function of the inverse of the absolute temperature, as in Figure 1.1. A linear dependence is obtained with a negative slope corresponding to $-E_{\mathrm{act}}/RT$.

Indeed, most chemical reactions between stable molecules slow to a halt at very low temperatures because the reactants lack the energy needed to surmount activation barriers. However, many reactions involving radicals do not possess a barrier along the minimum energy path (MEP) joining reagents to products over the potential energy surface (PES) that governs the reaction. These so-called barrierless reactions, which are often already very fast at room temperature, may remain rapid or even become faster as the temperature drops[2] down to the very low temperatures prevailing in extraterrestrial atmospheres such as that of Saturn's giant moon Titan (*ca.* 70–150 K)[3] or interstellar clouds (ISCs; *ca.* 10–100 K).[4,5] The chemistry of cold ISCs, including regions where stars and planetary systems form, was once thought to be completely dominated by ion–molecule reactions, which are barrierless owing to strong attractive forces. However, in no small measure due to the measurements described in this chapter, it is now recognized that neutral–neutral reactions play an important role in such environments,[4,5] and it is on this class of reactions that we focus our attention.

A wide range of experimental techniques exists for studying reactivity at low and ultra-low temperatures, as can be seen in the other chapters of this book. However, many techniques do not enable the measurement of

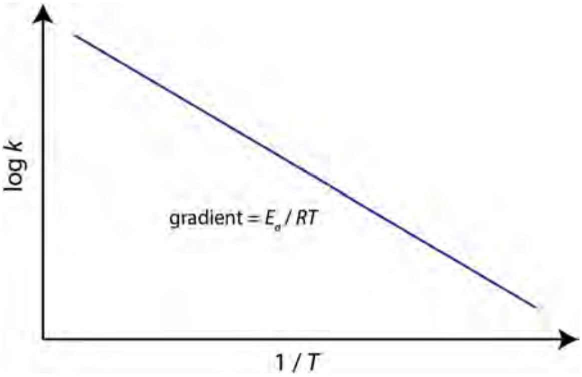

Figure 1.1 A plot of the log of the rate constant k against the inverse of temperature, commonly known as an Arrhenius plot, yields a characteristic linear dependence with a negative slope for reactions with a barrier and positive activation energy E_{act}.

absolute rate constants at low temperatures. In chemical kinetics, the principal method used to do this is based upon the use of so-called pseudo-first-order conditions, where for a bimolecular reaction A + B → products, the rate constant is determined by placing one of the two reagents (usually the most stable one) in large, known excess, and following the time-dependent concentration of the other reagent concentration. Because under these conditions the concentration of one reactant, in the present example reactant B, can be assumed to be constant, the standard second-order reaction rate eqn (1.3)

$$\frac{\mathrm{d}[\mathrm{A}]}{\mathrm{d}t} = -k\,[\mathrm{A}]\,[\mathrm{B}] \tag{1.3}$$

then reduces to the pseudo-first-order eqn (1.4) when $[\mathrm{B}] \gg [\mathrm{A}]$, with $k_{1\mathrm{st}} = k[\mathrm{B}]$:

$$\frac{\mathrm{d}[\mathrm{A}]}{\mathrm{d}t} = -k_{1\mathrm{st}}\,[\mathrm{A}]. \tag{1.4}$$

This technique effectively *isolates* the elementary reaction under study from other cross-reactions or self-reaction of the minority reagent A, and yields first-order exponential decays of [A] (or something directly proportional to it) which are analysed to yield values of $k_{1\mathrm{st}}$ as a function of co-reagent concentration [B]. An important advantage of this technique is that knowledge of the absolute concentration of A is not required. A plot of $k_{1\mathrm{st}}$ as a function of [B] should yield a linear graph with slope k, the required bimolecular rate constant. Variants on this methodology exist, notably the use of flow-tube and relative rate techniques, but in essence all are based on this method. Knowledge of the absolute concentration of the B co-reagent enables the determination of an absolute rate constant, which is useful for comparison with theoretical calculations as well as for input to models of gas-phase chemical environments.

The determination of absolute rate constants for gas-phase reactions at temperatures much below 200 K is very difficult, principally owing to condensation on the cold walls of the reactor, such that maintaining a sufficiently high and known concentration of the more abundant reactant (B in the example above) becomes a problem. The CRESU technique,[6–8] which is the subject of this chapter, solves this by creating a wall-less flow of cold gas by expansion through Laval nozzles. (CRESU is a French acronym standing for *cinétique de réaction en ecoulement supersonique uniforme*, or reaction kinetics in uniform supersonic flow). Using this method, many neutral–neutral reactions have been found to have rate constants that either remain very fast or even increase as the temperature falls below 300 K, down to values as low as 6 K.

In the case of ion–molecule reactions, fairly simple considerations involving capture on long-range potentials dominated by electrostatic interactions enable, in the vast majority of cases, a fairly reliable theoretical estimate of the overall temperature-dependent rate constant $k(T)$, even if branching into individual product channels remains an important subject for investigation. This is not, however, generally the case for neutral–neutral reactions which show more subtle effects in the temperature dependence of their overall rate constants.

Figure 1.2 shows three general cases for exothermic bimolecular reactions. The first case (a) illustrates a reaction with a substantial barrier caused by the necessity to break chemical bonds. The upper panel schematically represents the potential energy (the stored internal energy) of the system as the reaction takes place, as a function of the progress of reaction (the reaction coordinate), while the lower panel shows what an Arrhenius plot for such a reaction might look like. The reaction slows down rapidly as the temperature drops (towards the right of the plot). While roughly linear, a slight curvature is expected and is more evident at lower temperatures. The curvature is on account of the fact that the pre-exponential A factor is actually slightly temperature dependent[9] and the occurrence of quantum mechanical tunnelling, which enables the system to cross through the barrier to reactants at energies below the summit of the barrier. If both reactants are radicals, for example CN and O_2,[8] then there may be no barrier on the potential energy curve, as shown schematically in Figure 1.2(b). The potential curve displays a deep well as the unpaired electrons on each radical combine to form a chemical bond. In this case the reaction generally becomes faster as the temperature *drops*, as depicted in the lower panel of Figure 1.2(b). In fact, not only reactions between two radicals, but also reactions between radicals and closed shell molecules have been shown to be rapid. One of the earliest reactions to be studied at very low temperatures by the CRESU technique, $CN + C_2H_6 \rightarrow HCN + C_2H_5$,[10] showed a behaviour which is in some ways a combination of the two 'extremes' represented by Figure 1.2(a) and (b). At high temperatures it displays positive activation energy, but as the temperature decreases the rate constant passes through a minimum and then increases by almost an order of magnitude between 200 K and 23 K. This behaviour is characteristic of a system represented schematically in the upper panel of Figure 1.2(c), with an initial relatively weakly bound complex, which then goes on to cross a potential barrier to proceed to products. The interplay between the formation and redissociation of the initial complex *versus* subsequent crossing of the barrier has been invoked to explain the observed behaviour.[11,12] Further experimental and theoretical studies have shown that many radical–molecule reactions fall into this same category, but the minimum in the rate constant is not always observed in the temperature range of existing measurements as it depends strongly on the interplay between the initial well depth and subsequent barrier height as represented by the red arrows in the upper panel of Figure 1.2(c).

The temperature dependence of neutral–neutral chemical reactions down to very low temperatures is controlled as we have seen by a subtle interplay of barrier heights (and associated entropic effects) as well as the possible effects of quantum mechanical tunnelling in the case of relatively small barriers. Measurements of low-temperature rate constants provide therefore an exacting challenge both for quantum chemical calculations of *ab initio* PESs as well as for quantum dynamical scattering calculations or other theoretical

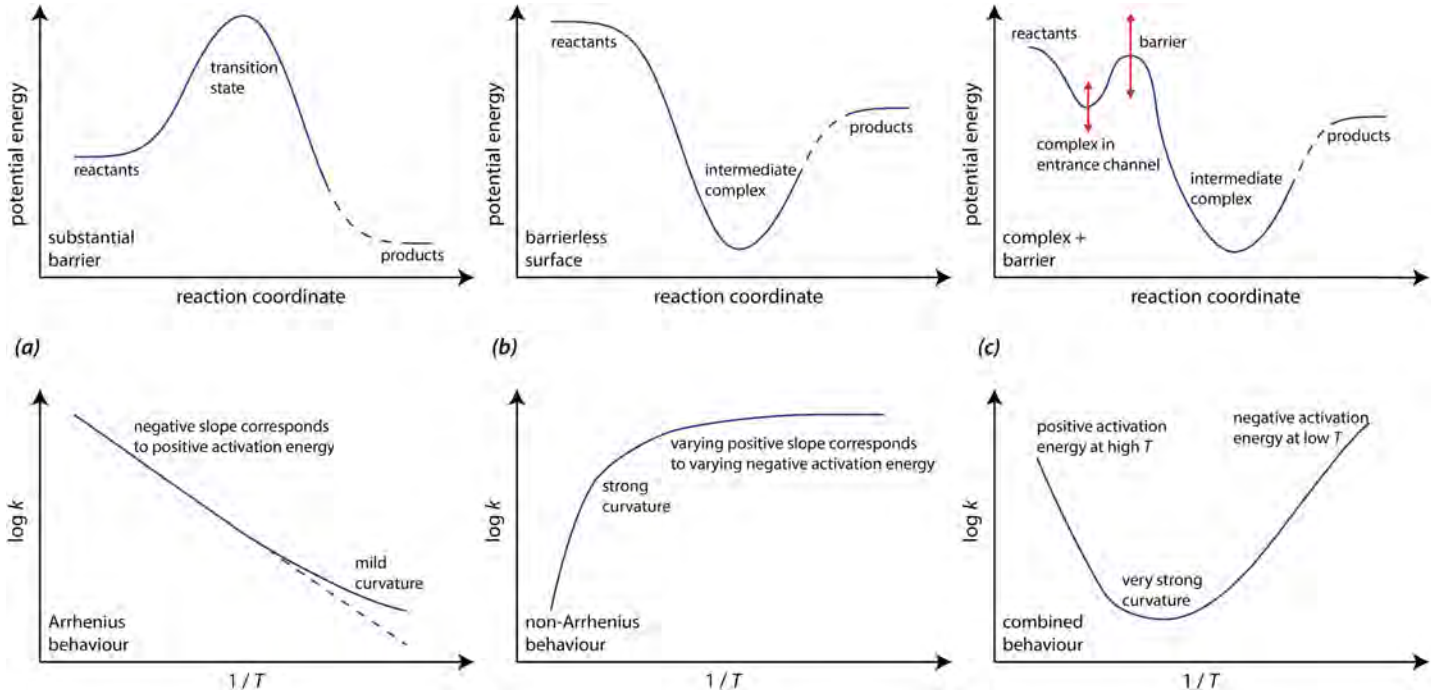

Figure 1.2 Schematic representations of the potential energy as the reaction takes place (*upper panels*) and the likely appearance of Arrhenius plots (*lower panels*) for three representative types of exothermic bimolecular reactions: (a) A reaction with a substantial barrier, which adheres approximately to the Arrhenius equation, though showing some non-linearity over a wide temperature range owing to a number of factors including quantum-mechanical tunnelling; (b) A reaction with no barrier, showing strongly non-Arrhenius behaviour; and (c) A reaction passing through an initial transient weakly bound complex and then over a barrier (which may or may not be above the reagent energy): the reaction adheres to the Arrhenius equation only at higher temperatures. Adapted by permission from Macmillan Publishers Ltd: *Nature Chemistry* (ref. 49), copyright (2013).

methods such as transition state theory designed to provide reaction rate constants.

Cryogenically cooled cells have been used to provide reaction rate constants in a few favourable cases down to below 100 K,[13] especially where the co-reagent is not easily condensable, as is the case for O_2. Studies of collisional energy transfer with bath gases such as He or H_2 also fall into this category, and the collisional cooling technique invented by Willey and De Lucia,[14,15] and later adapted and renamed buffer gas cooling by Doyle *et al.*,[16] has been used to obtain information on rotational energy transfer below 5 K in such cases: however, its application to date has been limited to inelastic collisions.

In order to investigate the kinetics of condensable species at very low temperatures it is necessary therefore to use expansion-based cooling methods. While free jet expansions and molecular beams have been used with great success in spectroscopy to prepare rotationally cold samples of isolated molecules, their use for the study of cold bimolecular reactions is limited by the very low densities and strong density gradients which result in a loss of the local thermodynamic equilibrium (non-Boltzmann distributions over rotational states, for example) and a lack of collisions within the expansion. The CRESU technique was originally invented by Rowe, Marquette, and co-workers[6,7] to study ion–molecule reactions by using a special type of expansion technique, which maintains thermalization at all times. The next section describes this technique in detail, after which a number of case studies will be detailed to illustrate its application to problems in low-temperature chemical kinetics.

1.2 The CRESU Technique

1.2.1 Uniform Supersonic Flows

When performing reaction rate measurements, as explained in the previous section, it is essential to know the absolute concentration of at least one of the reacting species. A common means of cooling a gas-phase reactor is to cool down the walls of the system by circulating a coolant or cryogen in a double-walled jacket around the gas-phase (slow) flow tube.[17] However, the vapour pressures of most molecular species of potential interest for low-temperature chemistry, including hydrocarbons and many others, shrink to a negligible level at temperatures below 200 K, and so such species will condense on the walls of the reaction vessel. Even if some reagents can be introduced *via* heated injectors far away from the walls, their concentration will neither be homogeneous in the reaction zone, nor able to be easily determined. This means that cooling *via* the walls of the reaction cell is not a viable method for (very) low-temperature kinetics, and we must find another way to cool down the reactant species.

The most widely used technique for generating cold gas-phase molecules in chemical physics experiments is by expansion from a very high-pressure reservoir through a small orifice to a very low-pressure chamber. By this free jet expansion technique a very high degree of cooling can be achieved, and subsequent passage *via* an appropriate skimmer can yield molecular beams where the internal rotational and translational temperatures can be of the order of 1 K or even well below. Such molecular beams have been used for example in the spectroscopic observation of the helium dimer at a translational temperature of 1 mK,[18] as well as in studies of reactivity by the use of the crossed molecular beam technique.[19] However, their use in low-temperature chemical kinetics is limited by the very strong density gradients and loss of local thermodynamic equilibrium, with non-Boltzmann rotational distributions and out-of-equilibrium translational temperatures, linked to the very low rate of collisions in such beams. This severely limits the use of these environments for kinetics studies especially of neutral–neutral reactions, where it is necessary to establish thermal equilibrium after, for example, photolytic generation of a radical reagent, on a timescale that is short compared to reaction. These two requirements—expansion cooling to enable the rapid generation of highly supersaturated gas samples, and reduction of the strong density gradients associated with uncontrolled free jet expansions to achieve a higher density homogeneous environment where local thermodynamic equilibrium can be maintained by frequent collisions—have led to the use of uniform supersonic expansions in kinetics applications.

Laval nozzles, described in 1888 by Gustaf de Laval, are axisymmetric nozzles consisting of a convergent section followed by a divergent section. They have found application in the generation of supersonic flows, notably for rocket motors. A Laval nozzle can be used to expand any gas and generate a supersonic expansion.

The action of a Laval nozzle on a gas flowing through it is a two-stage process. In the convergent section of the nozzle (see Figure 1.3), the gas is accelerated since the cross-section becomes smaller as the gas moves towards the exit (but the gas is not compressed). If the gas flow is adequate

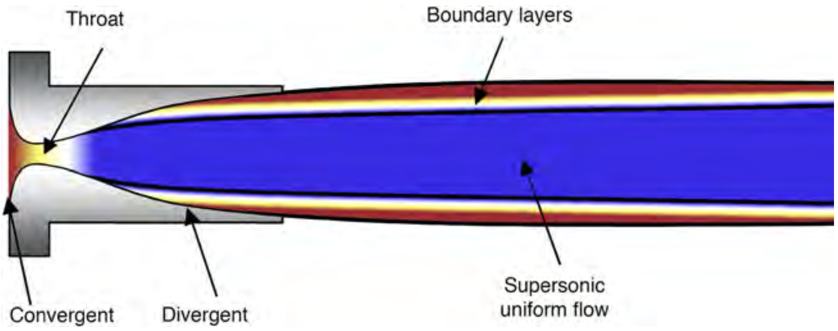

Figure 1.3 Schematic Laval convergent-divergent nozzle temperature map. Initial (reservoir) temperature in red (usually 298 K). Final (uniform supersonic flow) temperature in blue (typically 20–200 K).

for the nozzle, the gas reaches a Mach number of 1 at the throat. The gas further expands in the divergent section of the nozzle and reaches higher Mach numbers. The adiabatic expansion taking place through the nozzle reduces the temperature and density of the gas, while raising the velocity. If proper conditions are met, the flow is collimated and propagates along a cylindrical trajectory. If the pressure of the gas inside the flow is too high or too low, the flow is over-expanded or chocked and shockwaves will appear. This is to be avoided for a reaction rate study, since a local compression will be induced, changing the flow properties, and consequently the physical conditions encountered by the reactants.

In a Laval nozzle, the flow is compressible. It is possible to apply a variation of Bernoulli's equation, taking into account enthalpy and potential energy. However, the nozzle size is small (gravity effects are negligible) and the flow is isentropic. Thus, we can apply the following equations directly in such a nozzle.

$$C_\mathrm{p} T_\mathrm{flow} + \frac{v_\mathrm{flow}^2}{2} = C_\mathrm{p} T_0 + \frac{v_0^2}{2}, \tag{1.5}$$

$$PV^\gamma = \text{ constant}, \tag{1.6}$$

where C_p is the specific heat capacity at constant pressure, v the fluid velocity, T the fluid temperature, V the occupied volume, and γ the ratio of specific heat capacities, defined by $\gamma = C_\mathrm{p}/C_\mathrm{v}$, where C_v is the specific heat capacity at constant volume. The "0" indices refer to reservoir values (static gas), while "flow" indices can refer to any point in the flow.

In a CRESU experiment, the nozzle is mounted on a reservoir whose volume is large compared to the nozzle's internal volume. Because of this, the fluid velocity in the reservoir, v_0, is considered to be negligible compared to the speed in the Laval nozzle flow, v_flow. The Mach number, introduced before, is the ratio of flow speed to the speed of sound in the same fluid. It is important to remember that the speed of sound is influenced by the mass density of the medium (the higher the density, the higher the speed). The Mach number M is defined as

$$M = \frac{v}{a} \text{ with } a = \sqrt{\frac{\gamma R T}{M_\mathrm{m}}} \tag{1.7}$$

with R being the gas constant ($R = 8.314\ \mathrm{J\ K^{-1}\ mol^{-1}}$), T the fluid temperature, and M_m its molar mass. For an ideal gas:

$$C_\mathrm{p} - C_\mathrm{v} = R. \tag{1.8}$$

By substituting in Bernoulli's equation, we obtain

$$T_\mathrm{flow} = T_0 \left(1 + \frac{\gamma - 1}{2} M^2\right)^{-1}. \tag{1.9}$$

To obtain conditions suitable for reaction rate measurements, the flow needs to be collimated, that is, the pressure in the flow has to be equal to the pressure outside the flow (in the chamber for a CRESU experiment).

The nozzle is usually designed for use with a certain gas, and specific temperature and density parameters. When these conditions are respected, a low-temperature, uniform, supersonic, dense flow is produced.[6]

In reality, when constructing a Laval nozzle for any kind of experiment or application, certain points must be taken into account. The fluid viscosity is never zero and a small heat exchange with outer layers occurs. Thus, the process is not strictly adiabatic. Furthermore, an inverse solution of the Navier–Stokes flow equations is not analytically possible, but a numerical solution can be found using a perturbation method.[6] This is based on initial assumptions of an ideal fluid, with no viscosity and no heat exchange. It is then necessary to take into account two effects:

- the walls of the nozzle are at a fixed temperature (usually ambient temperature);
- the non-zero fluid viscosity imposes a velocity of 0 at wall contact, with a gradient of speed orthogonal to flow direction.

This allows the computation of a secondary flow, non-isentropic, of thickness δ_1, a layer of gas with a velocity of 0 at wall contact and with an increasing speed as distance increases. Physically it corresponds to the distance the wall has to be moved to keep a constant mass flow of fluid. Between the wall and the isentropic core is a layer where isentropicity is not achieved, the boundary layer of thickness δ in Figure 1.4.

The smaller the size of the boundary layer, the better the flow quality, since the isentropic core is the desired part of the flow. The Reynolds number Re is a good indicator of the flow quality. The Reynolds number, for a flow, is a non-dimensional quantity equal to the ratio of inertial forces to viscous forces. Viscous forces here are the actions of nozzle wall on the flow, and inertial forces are acquired by pressure differences of the fluid, converted as kinetic energy. The Reynolds number is given by

$$R_e = \frac{\rho v L}{\mu} \quad \text{with} \quad \frac{\delta}{L} \propto \frac{1}{\sqrt{R_\mathrm{e}}}, \tag{1.10}$$

where v is the flow velocity, ρ the fluid volumetric mass, L a characteristic length (uniform flow length for a CRESU experiment) and μ the dynamic

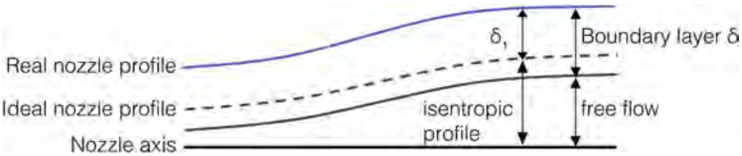

Figure 1.4 Real and ideal nozzle profiles, with flow left to right. The thickness of the isentropic core can be a few millimetres in radius (below 40 K) or as high as 2 cm radius at 200 K. The boundary layer thickness is typically the same order of magnitude as the isentropic core.

viscosity of the fluid. If the Reynolds number is low, the boundary layers are small compared to flow length. A good flow will therefore tend to be associated with a higher Reynolds number. Typical dimensions of Laval nozzles used in the CRESU technique are of the order of 20 cm long with a throat radius ranging between 2–3 mm and 2–3 cm. At their exit typical Laval nozzles can open up to a radius of 2–4 cm.

When fabricating a nozzle for an experiment, the critical part is the precision reached at the throat during the machining process. Any significant imperfections can cause serious perturbations to the subsequent uniform supersonic flow. Conditions for its use (pumping capacity, reservoir pressure, gas flow) are dictated by the laws of fluid mechanics, which are solved to generate a profile (radius R as a function of axis position z). Mechanical constraints further impose a certain minimal length and throat size. After the nozzle is constructed, it must be tested to measure the real specifications, usually close to theoretical calculations with any differences attributable to slight imprecisions in the machining process. Imperfection in the construction of the nozzle will result in a temperature and/or density differing from the design values, and an additional presence of oblique shockwaves (see Figure 1.6). These shockwaves have a negative influence on the uniformity of the density profile, and result in a larger standard deviation of the temperature along the flow.

The best way to test a nozzle is to use it in real conditions and sample the generated flow with a Pitot probe (Figure 1.5).

A Pitot probe is a hollow tube inserted inside the flow, parallel to its propagation. The impact of the flow on the tip of the probe creates a detached shockwave at the insertion point, and this “impact pressure” is measured by a pressure sensor at the other end of the tube. The impact pressure combined with the nature of the gas and the reservoir pressure can be used to deduce the flow characteristics. The impact pressure (P_i) and the flow pressure (P_f) are linked by a relation involving the Mach number M:

$$P_\mathrm{i} = P_\mathrm{f}\left(\frac{\gamma+1}{2}\right)^{\frac{\gamma+1}{\gamma-1}} M^{\frac{2\gamma}{\gamma-1}}\left(\gamma M^2 - \frac{\gamma-1}{2}\right)^{\frac{1}{1-\gamma}}. \qquad (1.11)$$

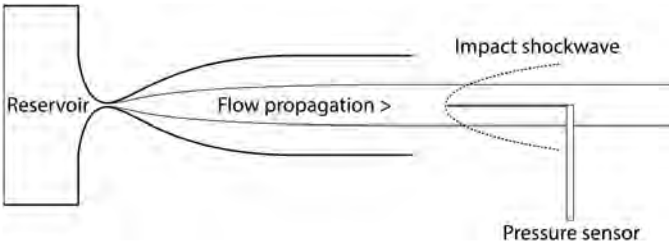

Figure 1.5 Pitot impact pressure measurement principle. A Pitot tube (a thin tube) is inserted facing opposite to the flow direction. A detached shockwave forms in front of it, and the impact pressure behind the shockwave is directed to a sensor. Another sensor monitors the reservoir pressure.

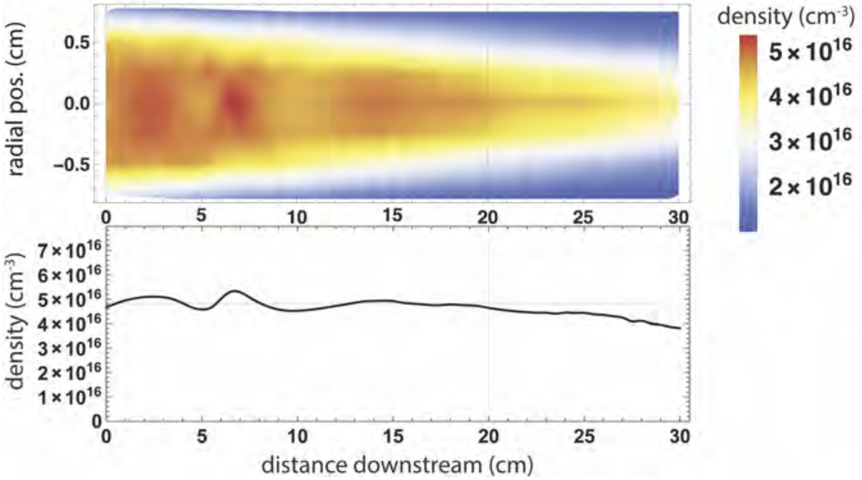

Figure 1.6 Density map (molecule cm^{-3}) (bottom) of a nozzle yielding a 23 K He flow for the CRESU experiment at the Institut de Physique de Rennes, and (top) a one-dimensional extract along the axis $r = 0$. Note how as the flow progresses, the boundary layers progressively reduce the size of the isentropic flow core, and the oblique compression shockwaves at downstream positions 5 cm and 10 cm. These shockwaves are caused by a slight difference in pressure between the flow and the chamber.

Because the core of the flow, where the probe is inserted, is isentropic, the impact pressure (P_i) can be expressed as function of the reservoir pressure (P_r):

$$P_\mathrm{i} = P_\mathrm{r}\left(\frac{(\gamma+1)M^2}{(\gamma-1)M^2+2}\right)^{\frac{\gamma}{\gamma-1}}\left(\frac{\gamma+1}{2\gamma M^2-\gamma+1}\right)^{\frac{1}{\gamma-1}}. \tag{1.12}$$

In order to obtain the flow characteristics, the reservoir pressure, temperature and mass flow must be kept constant, while measuring the impact pressure at every desired point. The equation can be solved for the Mach number (an analytical solution may not be possible, and numerical solution by an iterative algorithm is usually the preferred method). Once the Mach number for every point probed is obtained, the temperature, density, and flow velocity at this point are easily deduced. Sampling over a large number of points along the flow propagation axis gives proper information on the flow quality and properties. Figure 1.6 shows the result of a Pitot test yielding a density profile both along the central axis and as a 2D plot for a Laval nozzle giving an uniform supersonic flow at a temperature of 23 K, with a flow duration of about 100 µs. Resolutions are 5 mm along the flow axis and 1 mm in the radial direction. The Pitot tube has an internal diameter of 0.3 mm.

Such plots are used to determine the limits of potential reaction time under uniform flow conditions, as well as the average temperature and density, which are necessary for any reaction kinetics measurements. The reservoir temperature is obtained by the means of a thermocouple sensor (±0.1 °C) and the pressures are determined with an accuracy of ±0.1% on two independent sensors.

It should be noted that nothing requires the flow to be continuous, and indeed, several groups have developed pulsed versions of the CRESU technique, in order to reduce gas consumption. Pulsing can be done before the reservoir,[20–24] or between reservoir and nozzle.[25–27] Pulsing before the reservoir generally requires a rather small volume for the latter in order to ensure rapid filling, which can reduce the quality of the supersonic flow, as the gas is no longer static to a good approximation before entering the convergent section of the Laval nozzle. One solution to this problem is based on the use of high-force fast piezoelectric actuators to enable very fast high-throughput valves.[24] Alternatively, pulsing the flow just after the throat of the nozzle by means of a spinning disc valve gives superior performance, but at the cost of increased problems of wear on the necessary sliding seals.[25–27]

1.2.2 Kinetics Techniques in Combination with Uniform Supersonic Flows

A uniform supersonic flow can be thought of as essentially a flow tube without walls, in which reagents and precursors can be introduced at partial pressures in excess of their saturated vapour pressure at the temperature of the flow. In essence, any reaction kinetics technique that can be applied in standard room-temperature flow tubes stands a good chance of being applicable in uniform supersonic flows as well. As mentioned above, in order to apply the isolation method to study bimolecular reactions between neutral species, we need to ensure that one of the reagents is present in large and known excess, and then to record the concentration of the other, usually radical, species in a time-resolved fashion—though not necessarily on an absolute scale of density, as explained above. The most common method used to measure reaction rate constants in uniform supersonic flows has been the pulsed laser photolysis—laser-induced fluorescence (PLP-LIF) technique. Indeed, this was used for the first measurements of radical–molecule reaction rate constants in the CRESU technique,[8,10] and will be explained in detail below. Other reaction kinetics methods used in conjunction with the CRESU technique include the chemiluminescence marker technique for the study of C_2H and $C(^3P)$ reactions,[28,29] whereby a radical concentration is followed *via* a reaction yielding an excited-state fluorescing product, and mass-spectrometric sampling, employing the CRESU in fast flow-tube mode for time resolution of cluster formation.[30,31] Variants for the measurement of product-channel-specific rate constants are discussed later in the chapter.

In a CRESU apparatus, the reaction to be investigated has to be initiated for the study. When working on radicals, the most common way to do it is using pulsed laser photolysis (PLP), typically employing high-power UV pulsed excimer lasers operating at 193 nm (ArF) or 248 nm (KrF), or the fourth harmonic of an Nd : YAG laser at 266 nm.

Laser-induced fluorescence (LIF) is a technique of selective excitation by absorption of laser light of a specific wavelength and subsequent fluorescence detection of a species using a specific wavelength.[32,33] Most often it is based on the use of a tuneable dye laser or an optical parametric oscillator/amplifier (OPO/OPA). An electronic transition is usually targeted with visible/UV lasers. The excitation can be in resonance, that is, the de-excitation of the species will produce the same wavelength as the excitation, or non-resonant. In the latter case, typically the excited species will fluoresce to a higher vibrational level of the ground electronic state, which gives the possibility of filtering out the excitation light from the laser and selectively collect the fluorescence. If the experiment must be done in resonance, the best way to collect the light is to discriminate it geometrically or temporally from the source light. LIF is an extremely sensitive technique. A major drawback of LIF is the technical impossibility of scanning over a large range of wavelengths easily, as the light source has to be changed. A typical dye laser will, with one dye, reach a range of 20–40 nm in the visible, divided by two or three if using second- or third-harmonic generation. This means that the experimenter must already know what to look for when setting up the experiment. In the case of UV/visible wavelengths, mirrors must often be changed, which requires a new alignment procedure. For this reason, PLP-LIF is often used to track the decay of one of the injected species, rather than the appearance of products.

In the CRESU experiment, the pseudo-first-order-technique is used if possible.[34] This technique allows the measurement of a second-order rate constant with multiple first-order experiments, as described previously. A few μs (typical range 0–400 μs) after the photolysis pulse, the tuneable laser pulse excites the tracked species to probe its concentration. This causes fluorescence, which is collected by a photomultiplier tube that converts a light intensity into a measurable current, in a linear fashion. The resulting current is converted into a voltage which is integrated and digitized, and the integrated value plotted against the time delay. The pair of PLP and LIF laser pulses are repeated for a different time delay. With sufficient pairs of PLP-LIF pulses, a decay curve is obtained, which should be single exponential in the case of pseudo-first-order kinetics. With multiple pseudo-first-order experiments, it is possible to obtain the second-order rate constant of the reaction measured.

The PLP-LIF process is represented schematically in Figure 1.7. The following steps are repeated for each single point of a PLP-LIF decay:

- In the cold, uniform, supersonic flow, with typically 1% reactant and 0.01% precursor, we consider here an infinitesimal sample.

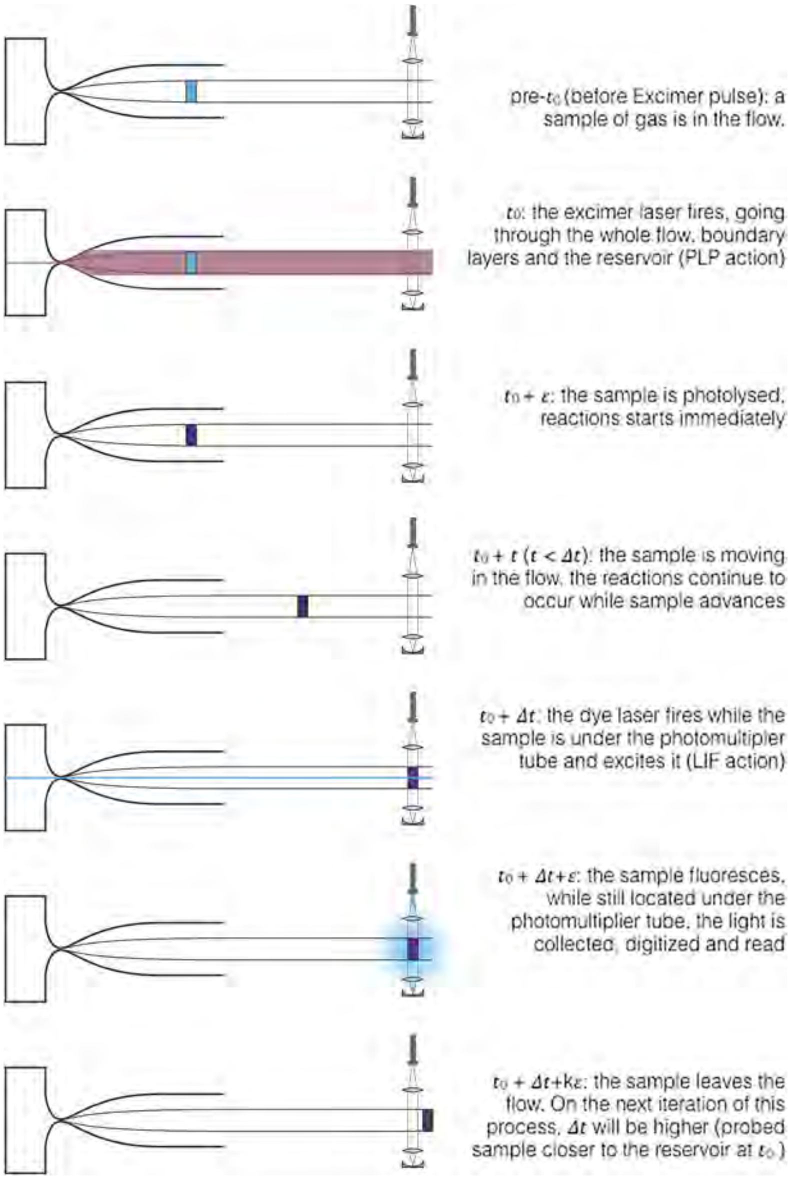

Figure 1.7 A schematic representation of the PLP-LIF technique implemented within a CRESU apparatus. Refer to the text for further explanations.

- PLP occurs, performed by an excimer laser or the fourth harmonic of an Nd : YAG laser. Bonds are selectively broken and the whole flow now contains radicals. PLP has a limited efficiency, defined by the absorption cross-section of the precursor at the PLP wavelength, the quantum yield for the formation of the radical species and the fluence of the laser. The reactive species is formed at strictly less than 0.01%

of the total flow density. Negligible heating of the flow occurs, owing to the high density of cold buffer gas present. This event corresponds to the start time t_0.

- Because the flow is dense, collisions quickly occur between newly formed radicals and species in the flow, statistically more often with carrier gas, which thermalizes the radicals. Reactive collisions occur when radicals encounter the reactant species (typically at 1% of the total flow density). This depletes the concentration of active species, while reactant species concentration remains quasi-constant. Minor reactions involve reactive species with its precursor (0.01%) and two reactive species together (extremely low probability).
- The whole flow, in particular the infinitesimal sample, advances towards the end of the supersonic beam, while reactions occur depleting the reactive species.
- After a time Δt the LIF pulse occurs, illuminating any reactant radicals still present in the flow, either over the whole flow, or—if the diameter of the laser beam is smaller—over a flow cylinder included in the flow.
- Excited reactive species fluoresce and emit light on a very short timescale (typically 10–100 ns half-life). All species in the flow fluoresce at the same time, but because the fluorescence is a very fast process compared to the movement of the species in the system, only species directly below the photomultiplier tube when the LIF pulse occurs are actually detected (even with a fast nozzle, the speed is usually less than 200 m s^{-1}, meaning that in 100 ns the flow advances by less than 0.2 mm). The collection area of the photomultiplier tube is a section directly in beneath it, a few centimetres wide in the CRESU. The fluorescence signal is usually collected *via* a gated integrator.
- The process is repeated for a different Δt (up to a maximum defined by the time taken for a sample of gas starting at the exit of the nozzle to reach the detection zone at the PMT), to construct the signal curve as a function of time, which should be an exponential decay. Fitting this curve gives the pseudo-first-order rate for that particular concentration of co-reagent.
- The whole cycle is repeated for differing co-reagent concentrations and the resulting second-order plot yields the rate constant for the reaction.

1.2.3 Limitations of the CRESU Technique

Limitations of the CRESU technique include a restriction to the measurement of relatively rapid reaction rates at low temperatures, and also the need for significant equipment and consumable resources.

Introduction of a reagent into the CRESU flow is usually restricted to a few percent of the buffer gas flow rate, as the nozzle and flow conditions are calculated using the characteristics (viscosity, molar mass, specific heat capacity) of the buffer gas. It may be possible under certain circumstances to recalculate nozzles and flow conditions for higher reagent proportions, though this will likely result in considerably different final temperature and density conditions in the uniform flow. Particularly at the lowest temperatures, the introduction of molecular co-reagents, especially those of higher mass and complexity, is likely to be limited by the onset of dimerization and subsequent formation of higher oligomers. For a typical uniform flow density of 5×10^{16} molecule cm^{-3} the maximum reagent concentration will not be more than 10^{15} molecule cm^{-3}, and this, combined with typical hydrodynamic flow times of the order of 200 μs at the lowest temperatures, means that the CRESU technique is best adapted for the study of relatively rapid reactions, with a lower limit of around 10^{-12} cm^3 molecule^{-1} s^{-1} in all but the most favourable cases.

The size of the apparatus is another significant constraint. Since Laval nozzles are usually designed to obtain a low pressure in the supersonic flow (around a fraction of a mbar) in order to avoid problems of reagent homogeneous condensation, large pumping capacities are necessary for the apparatus. Typically, studying binary reactions involving neutral partners, at temperatures as low as 15 K, requires pumping capacities of about 30 000 m^3 h^{-1}. An Olympic pool of standard dimensions has a volume of 2500 m^3. Hence, these pumps can empty the volume of gas that would fill an Olympic pool in just 5 minutes. The Rennes CRESU chambers are typically 0.5 m in diameter and 3 m long. However, if pressures of about 1 mbar are acceptable in the supersonic flow for the study of a given process (for example, if only reagent molecules containing a few atoms are to be used or higher temperatures are of interest), then a significant reduction in pumping capacity can be achieved at these higher chamber pressures, as is the case for the mini-CRESU that has been constructed at the Université de Bordeaux 1 by M. Costes and co-workers.[35] This apparatus, however, cannot reproduce temperatures lower than 50 K in the supersonic flow because of its limited pumping capacities. Another way to diminish significantly the size of a CRESU apparatus is to develop pulsed uniform supersonic flows, as mentioned above. Various types of pulsed CRESU apparatus have been developed in different laboratories, including our own, but are not the main subject of the current chapter.[20–27]

1.3 Case Studies

We now present a number of case studies drawn mainly from our own work to illustrate the wide range of applications of the CRESU technique in low-temperature chemical kinetics. It has long been known that reactions between two radical species are likely to have no barriers to reaction along the MEP (case b of Figure 1.2), and we start with the first neutral–neutral reaction between two unstable radicals studied by the CRESU technique, the reaction O + OH. We then go on consider reactions between radicals and molecules where the absence of a barrier to reaction is less obvious (case c in Figure 1.2), and illustrate this with a study of O(^{3}P) + alkene reactions. Finally, in our survey of basic bimolecular reaction types we illustrate the importance of quantum mechanical tunnelling in maintaining a rapid rate constant even at very low temperatures for reactions with a barrier (case a in Figure 1.2) by the study of the important interstellar reaction F + H_2. Following on from these prototypical reaction kinetics examples, we then illustrate wider applications of the CRESU technique to the study of the thermodynamics and kinetics of weakly bound species, and in the determination of product branching ratios by two different but highly complementary techniques.

1.3.1 Radical–Radical Reactions: $O + OH \rightarrow O_2 + H$

The first neutral–neutral reaction to be studied by the CRESU technique, CN + O_2,[8] was a radical–radical reaction, but molecular oxygen, albeit a diradical with a triplet ground state, is of course a stable gas and easily handled. In order to study reactions between two unstable radicals, one of the two must be generated in large and known excess, and with the high gas flows and lack of transverse diffusion mixing within the cold uniform supersonic flow this has proved challenging. The first such study was reported in 2006.[36] The $O(^3P_J) + OH(X^2\Pi_\Omega) \rightarrow O_2 + H$ reaction has been the subject of numerous experimental and theoretical studies. In the late 1970s and early 1980s, I. W. M. Smith's group measured the rate coefficient of this reaction using the discharge flow technique down to 250 K,[37] and then in the mid-1990s down to 158 K.[38] Subsequently a number of other experimental studies have been performed as well as numerous theoretical calculations, and references to some of this work may be found in Carty *et al.*[36] Based on this earlier work, astrochemical modellers had, by extrapolation from the lowest temperature values, been using a rate coefficient for this reaction at 10 K in excess of 10^{-10} cm^3 molecule^{-1} s^{-1}.[39] However, results from satellite observations[40–42] of the (very low) concentration of molecular oxygen in interstellar clouds have resulted in significant interest in this reaction. Viti *et al.* suggested that an activation energy $E_{act}/R = 80$ K would be necessary to explain the low abundance of O_2 in interstellar clouds, resulting in a rate coefficient at 10 K around four orders of magnitude below the previously assumed value. It was therefore decided to undertake the difficult task of measuring this rate coefficient at lower temperatures using the CRESU technique.

A novel VUV co-photolysis technique was chosen to generate the necessary concentrations of ground-state atomic oxygen and the low concentrations of OH radicals. Using Laval nozzles designed to work with N_2 buffer gas (see below) at temperatures down to 39 K, Carty *et al.*[36] introduced a mixture of known concentrations of molecular oxygen and trace quantities of water vapour into the supersonic flow. An F_2 excimer laser operating at 157 nm was then used to produce oxygen atoms by photolysis of molecular oxygen, and OH radicals *via* photolysis of water. At each O_2 concentration used, the fluence of the VUV laser was carefully measured *in situ* and this, coupled with knowledge of the O_2 photodissociation cross-section at 157 nm, enabled the calculation of the O atom concentration. The photodissociation of O_2 at 157 nm produces both $O(^3P)$ and $O(^1D)$ atoms, and so the use of N_2 as a buffer gas was essential in order to rapidly relax the excited-state $O(^1D)$ atoms to $O(^3P)$. This co-photolysis thus created the necessary pseudo-first-order conditions and the subsequent decay of OH radical concentration was followed by LIF using a second pulsed tuneable dye laser operating at 282 nm.

An example of the decay of OH radicals in the presence of oxygen atoms at 47 K is shown in Figure 1.8 along with the associated second-order plot. The results obtained required correction for expansion of the gas caused by absorption of the photolysis beam, as well as relaxation of vibrationally excited OH radicals by O_2 and N_2 during the reaction. Once these (relatively minor) corrections had been applied, the rate coefficient for the reaction between $OH(X^2\Pi_\Omega)$ and $O(^3P_J)$ shows no significant variation between 142 and 39 K with a value of $(3.5 \pm 1.0) \times 10^{-11}$ cm^3 molecule^{-1} s^{-1} through this range of temperature. This result is somewhat lower than the values reported earlier by Smith and Stewart,[38] but is in good agreement with the latest theoretical work, as reviewed recently by Teixidor and Varandas,[43] as shown in Figure 1.9.

1.3.2 Radical–Molecule Reactions—$O(^3P)$ + Alkenes

One of the most surprising results to come out of the early CRESU work on neutral–neutral reactions was a study on the reactions of the CN radical with a number of hydrocarbons, both unsaturated (C_2H_2 and C_2H_4) and saturated (C_2H_6).[10] Not only were the rate constants for these radical–molecule reactions all found to be fast at very low temperatures (down to 25 K), but the rate constant for the $CN + C_2H_6$ reaction was found to display a minimum with Arrhenius-type behaviour at higher temperatures, and barrierless-type behaviour at lower temperatures. This was understood in terms of the transient formation of a pre-reactive complex,[11] and subsequent passage over a barely submerged, but tight (*i.e.* low entropy) barrier,[12] corresponding to case c in Figure 1.2.

It was later understood that the temperature dependence of radical–molecule reaction rate constants is to a great extent determined by the height of this barrier, which results from avoidance of crossing between ionic and covalent potential curves. On this basis, together with an analysis of a large number of radical-unsaturated molecule reactions studied at very low temperatures, I. W. M. Smith *et al.*[44] proposed a second, semi-empirical method for deciding whether rate coefficients would be substantial at the temperature of ISCs, whereby, when the difference between the ionization energy of the molecular reagent (I.E.) and the electron affinity of the radical (E.A.), (I.E.—E.A.), is significantly greater than 8.75 eV, the reaction is likely to possess a 'true' barrier and will therefore become negligibly slow at 20 K. On the other hand, reactions with (I.E.—E.A.) $< \sim$8.75 eV are likely to be characterized by, at most, inner barriers that are submerged below the asymptotic

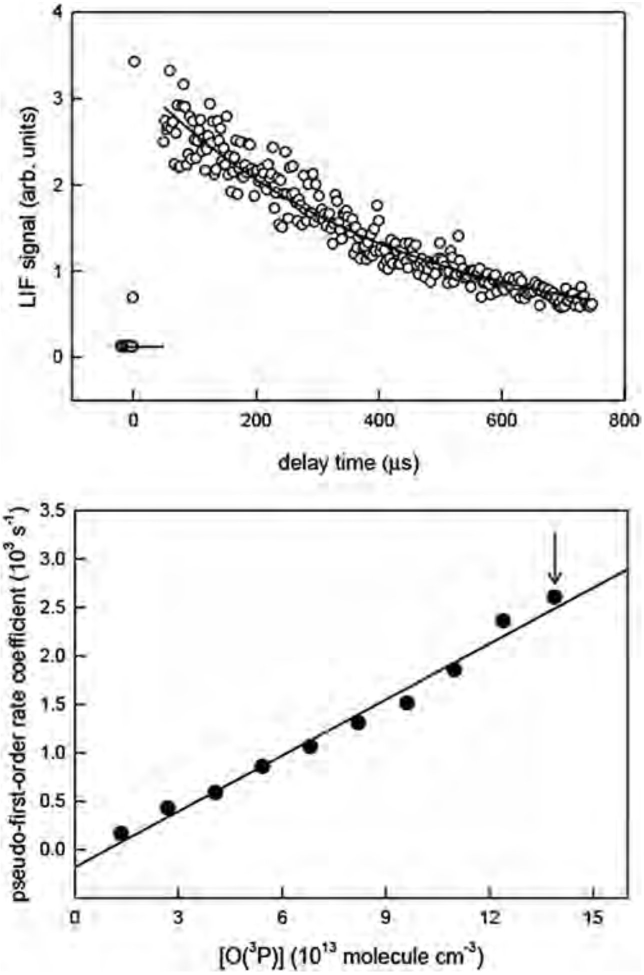

Figure 1.8 Experimental data for the O + OH reaction. *Upper panel:* LIF signals from OH at different delay times between the pulses from the photolysis and probe lasers at 47 K and [O(^{3}P)] = 13.9 × 10^{13} molecules cm^{-3}. *Lower panel:* Plot of the pseudo-first-order rate coefficients for decay of the OH concentration at 47 K plotted against the concentration of O(^{3}P) atoms, uncorrected for the heating/expansion effect mentioned in the text. The statistical errors are smaller than the size of the points. The arrow indicates the value of k_{1st} derived from the fit shown in the upper panel. Adapted with permission from ref. 36. Copyright 2006 American Chemical Society.

reagent energy, and therefore be rapid at 20 K and of potential importance in ISC chemistry. Smith *et al.* further pointed out that the reactions between ground-state oxygen atoms, O(^{3}P), with simple unsaturated hydrocarbons possess values of (I.E.—E.A.) that bridge the 'critical' value of 8.75 eV and would therefore provide an important test of their hypothesis.

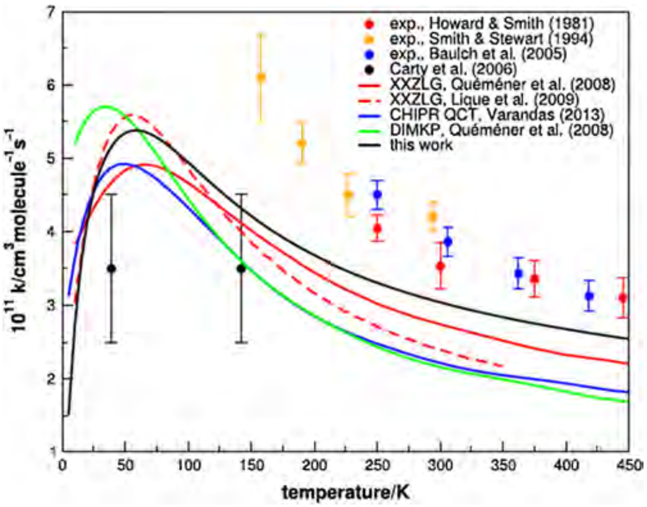

Figure 1.9 Rate constants for the reaction O + OH($v = 0$, $j = 0$) as a function of temperature: from Teixidor and Varandas[43] (solid black), and experimental (CRESU) data from Carty *et al.* (black filled circles). Other experimental (filled circles) and theoretical (lines) data are as described in Teixidor and Varandas.[43] Reprinted from M. M. Teixidor and A. J. C. Varandas, *J. Chem. Phys.*, 2015, 142, 014309, with the permission of AIP Publishing.

In order to test this proposal, we performed low-temperature measurements of the rate coefficients for these reactions, as reported in Sabbah *et al.*[45] O(^{3}P) atoms were generated in the cold CRESU flow *via* 355 nm laser photolysis of NO_2, and their concentration followed using chemiluminescence from excited NO_2*, formed in the association of O(^{3}P) with NO, as a 'marker' for the oxygen atom concentrations. As the NO concentration and the total pressure did not change during the reaction, the NO_2* fluorescence was proportional to the instantaneous O(^{3}P) concentration, which decayed exponentially as a result of reaction with the added alkene. Results were obtained in most cases down to 23 K or 27 K, except for the O(^{3}P) + ethene reaction, for which only an upper limit could be measured at 39 K. Sabbah *et al.*[45] also reported electronic structure calculations employing second-order multi-reference perturbation theory (CASPT2) to determine the inner barrier heights. For O + propene, the CASPT2-predicted barrier was adjusted downwards by 0.6 kJ mol^{-1}, to obtain optimum agreement with experiment. For consistency, this adjustment was applied to the other reactions as well. For the butene cases, this adjustment had an insignificant effect on the predictions. The experimental low-temperature data, high-temperature literature data from Cvetanovich,[46] and the theoretical calculations are all displayed in Figure 1.10. The experimental results can be seen to clearly fall into the three categories referred to above: O(^{3}P) + *cis*-, *trans*- and *iso*-butene possess fully submerged barriers, and display rapid rate coefficients with a negative temperature dependence at all temperatures. O(^{3}P) + ethene possesses a 'true' non-submerged barrier, and its rate coefficient falls below the minimum value usually measurable in the CRESU of *ca.* 10^{-12} cm^3 molecule^{-1} s^{-1} at 39 K. O(^{3}P) + 1-butene and O(^{3}P) + propene appear to fall into the category of a barely submerged inner barrier, and display the characteristic minimum first observed at low temperatures for the CN + C_2H_6 reaction. In all cases the calculations achieve a remarkably good agreement with experiment. In particular, the semi-empirical predictions of I. W. M. Smith *et al.*[44] are clearly supported by these data. All of the reactions possessing (I.E.—E.A.) < 8.75 eV are found to be rapid at low temperatures, and the two cases showing a turnaround from positive to negative temperature dependence as the temperature falls are identified by their values of (I.E.—E.A.) only slightly below this threshold (8.09 and 8.27 eV for O(^{3}P) + 1-butene and O(^{3}P) + propene respectively).

It is interesting to ask to what extent these predictions can be applied more widely. We can compare the value of (I.E.—E.A.) for the reaction O(^{3}P) + *cis*-butene, 7.65 eV with that for the reaction CN + C_2H_6, 7.66 eV. The former

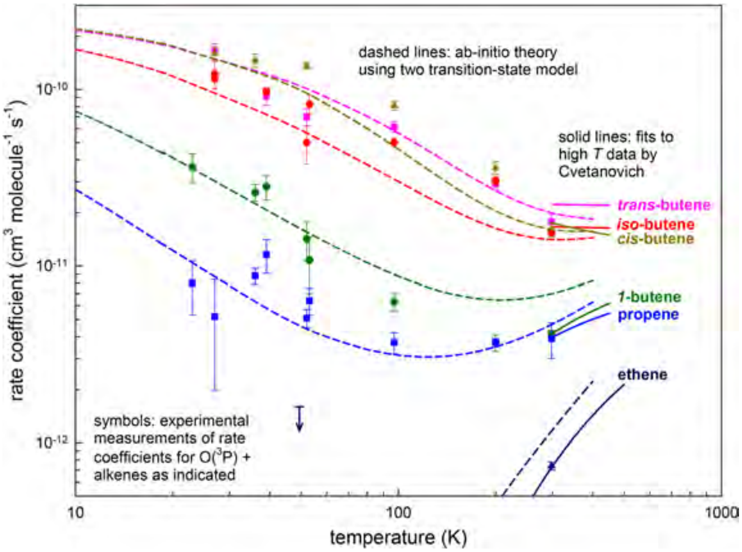

Figure 1.10 A plot of rate coefficients as a function of temperature for a range of O(^{3}P) + alkene reactions on a log–log scale. The points show the experimentally determined values of the rate coefficients, while the dashed lines show the results of the theoretical calculations described in the text.[45] The solid lines to the right of the diagram represent the Arrhenius expressions recommended by Cvetanovic[46] to fit kinetics data between 300 and 700 K.[45] Adapted from H. Sabbah, L. Biennier, I. R. Sims, Y. Georgievskii, S. J. Klippenstein and I. W. M. Smith, *Science*, 2007, **317**, 102–105. Reprinted with permission from AAAS.

clearly has a fully submerged barrier, while the latter's kinetic behaviour places it into the same category of a barely submerged barrier displayed by the O(^{3}P) + 1-butene and O(^{3}P) + propene reactions. Clearly, the rule is less than perfect outside of a homologous series of reagents such as O(^{3}P) + alkenes, but it should still prove very valuable for reactions where (I.E.—E.A.) is either much greater than 8.75 eV (*e.g.* CN + H_2, where I.E.—E.A. = 11.56 eV, negligibly slow at low temperatures), or much less than this value (*e.g.* CN + C_2H_2, where I.E.—E.A. = 6.65 eV, rapid at low temperatures). Furthermore, Sabbah *et al.* proposed a refinement to the rules of I. W. M. Smith *et al.*: compare theoretical and experimental values of the room-temperature rate coefficient in order to estimate the barrier height at the inner transition state, and when this barrier is submerged one can reasonably expect the reaction to be rapid at the low temperatures of ISCs. However, the most important conclusion that can be drawn is that both the empirical and semi-empirical rules proposed by I. W. M. Smith *et al.* and based respectively on kinetic behaviour at room temperature and above, and on the values of (I.E.—E.A.), appear to perform well and provide a firm basis for predicting the low-temperature rate coefficients for (as yet) unmeasured reactions.

1.3.3 Reactions with Barriers and the Role of Tunnelling—The F + H_2 Reaction

The first reactions to be studied extensively by the CRESU technique were characterized by barrierless potential surfaces, or at least by the absence of absolute barriers along the MEP for reaction. As explained in the previous section, the presence of submerged barriers does, however, exert a strong influence on the temperature dependence of rate constants for radical–molecule reactions. Typically, reactions with significant barriers are often relatively slow at room temperature (rate constants of 10^{-12} cm^3 molecule^{-1} s^{-1} or less) and this was thought to preclude their measurement by the CRESU technique, as explained earlier (Section 1.2.3). For the most part, such reactions were thought to be uninteresting for astrochemical applications as such reactions would not contribute significantly to low-temperature interstellar chemistry in comparison with other fast ion–molecule and neutral–neutral barrierless processes. However, reactions involving hydrogen are a significant exception to this rule. In the first place, in dense interstellar clouds, molecular hydrogen dominates all other molecular species by a factor of at least 10^4, and so even relatively slow reactions involving molecular hydrogen can be of great importance. Secondly, reactions with activation barriers that involve H-atom transfer can still have significant rate constants at very low temperatures due to quantum mechanical tunnelling. Examples of the latter effect studied in uniform supersonic flows include the OH + CH_3OH reaction, where a significant enhancement in rate constant was found to take place at low temperatures owing to the formation of a pre-reactive complex followed by tunnelling through a barrier enhanced by long complex lifetimes at low temperatures,[47–50] and the $F + H_2$ reaction which will be detailed in this case study.

The $F + H_2 \rightarrow HF + H$ reaction (where the reagents and products are in their electronic ground states) is a benchmark for both quantum scattering calculations and reaction dynamics experiments, and has been the subject of numerous experimental and theoretical studies.[51] It is also of great interest for interstellar chemistry as it is essentially the sole process responsible for the creation of interstellar HF, which was first observed in 1987 by the Infrared Space Observatory in absorption on its $J = 2 \leftarrow 1$ transition at a frequency of 2.463 THz. However, it was not until the advent of the Herschel Space Observatory in 2010 that HF was detected very widely by the HIFI (Heterodyne Instrument for the Far Infrared) spectrometer on the $J = 1 \leftarrow 0$ transition at a frequency of 1.232 THz.[52] HF is of significant interest as it acts as a tracer for the majority species in interstellar clouds, H_2, which has no dipole moment and is thus difficult to detect directly. Because of the unique thermochemistry of HF,[52] it constitutes the dominant reservoir of interstellar fluorine.

In order to relate the observed densities of HF to H_2, it is essential to know the absolute magnitude of the rate constant of the $F + H_2$ reaction down to the temperatures of ISCs, 10–100 K. As a reaction with a significant, if relatively small barrier ($E/R \cong 800$ K) its rate constant had not been measured below 190 K before the study reported here, and was found to decrease strongly below room temperature.[53] However, it was realized that quantum mechanical tunnelling would increasingly dominate as the temperature falls, and a range of theoretical determinations were performed to calculate the low-temperature rate constant. These calculations predict very different values between 4×10^{-14} and 2×10^{-12} cm^3 molecule^{-1} s^{-1} in the 5–10 K temperature range.[54] However, the highest-level calculations by Zhu *et al.*[55,56] employed by Neufeld and Wolfire[57] in their interstellar fluorine chemical model implied likely rate constants below 10^{-12} cm^3 molecule^{-1} s^{-1} at low temperatures, below the normal limit for CRESU measurements.

The lower limit for measurable rate constants in the CRESU of *ca.* 10^{-12} cm^3 molecule^{-1} s^{-1} can be extended to *ca.* 10^{-14} cm^3 molecule^{-1} s^{-1} if, instead of introducing the molecular co-reagent in trace concentrations (of the order of 1%), the reagent is used as the buffer gas for the uniform supersonic flow. The use of molecular hydrogen as a buffer gas does, however, present certain difficulties owing to its slow rotational relaxation and in particular the ‘freezing out’ of its rotation below room temperature, resulting in a transition of its ratio of specific heat capacities, γ, from its diatomic value of 7/5 near room temperature to the value for a monatomic gas of 5/3 below about 80 K. As γ is a key parameter in relation to uniform supersonic flows, this constituted a significant problem, and it was decided to pre-cool the reservoir and Laval nozzle with liquid nitrogen. At 77 K H_2 rotation is essentially frozen out, and only $J = 1$ and $J = 0$ levels are populated with an *ortho*-H_2/*para*-H_2 ratio of 3 : 1 (so-called normal hydrogen).

Laval nozzles were fabricated and characterized in this way for temperatures of 5, 11, and 20 K.[54]

The reaction was studied by introducing a small concentration of molecular fluorine F_2 into the cold H_2 flow, and the F_2 was photolyzed using a 248 nm KrF excimer laser to yield atomic fluorine $F(^2P)$. Detection of atomic fluorine by LIF is difficult (requiring short wavelengths which would preclude the use of windows), and so the reaction was monitored *via* the appearance of the H-atom product, which was detected by pulsed VUV LIF at 121.6 nm. Measurements were carried out at room temperature and 77 K in subsonic flows, and at 5, 11 and 20 K in supersonic flows. An example H-atom growth and decay curve is shown in Figure 1.11.

A prompt signal, which was found to be due to reaction within $F_2 \cdots H_2$ complexes formed at small concentrations during the Laval nozzle expansion, was found to be present at 20 K (see Figure 1.11), and this increased in importance at 11 K, rendering the determination of the rate constant less precise. At 5 K this signal was so strong that it precluded any determination of the gas-phase bimolecular rate constant.

In parallel to the experimental measurements, Lique and Alexander carried out non-Born–Oppenheimer quantum scattering calculations on their new hybrid Li–Werner–Alexander–Lique (LWAL) PES. The results of these calculations (with and without non-Born–Oppenheimer effects) are compared to the experimental results in Figure 1.12.

As can be seen, the experimental results confirm the accuracy of the new non-Born–Oppenheimer calculations of Lique and Alexander. These

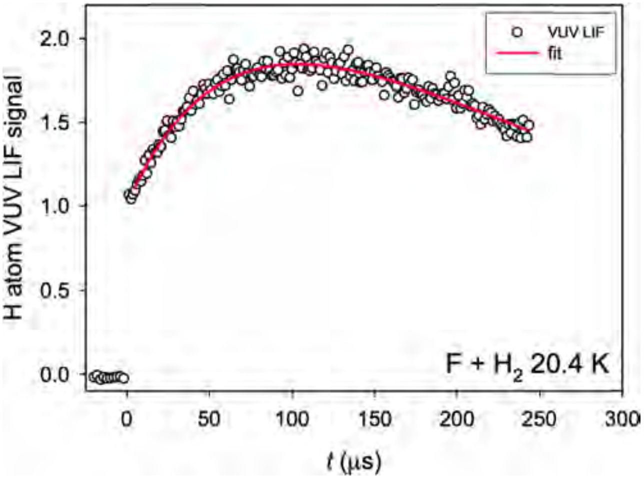

Figure 1.11 H-atom LIF growth and decay curve, monitored by H-atom VUV LIF (in arbitrary units) at a temperature of 20.4 K (unfilled circles). The data are fitted to a growth and decay function taking into account reaction and diffusion. Note the prompt signal at zero time. Adapted from Tizniti *et al.*[54]

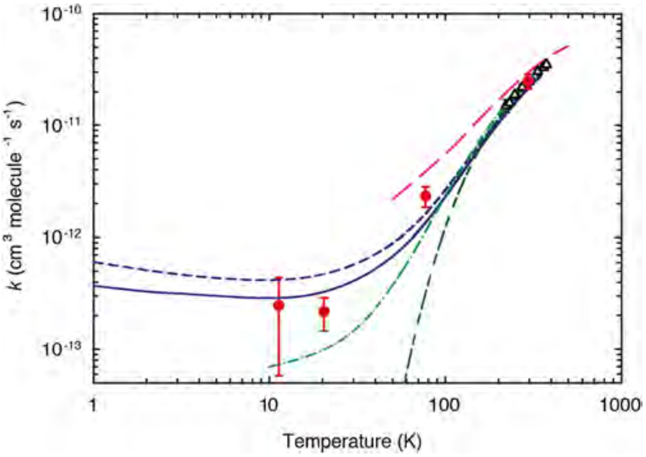

Figure 1.12 A comparison of rate coefficients k for the $F(^2P_J) + n\text{-}H_2 \rightarrow HF + H$ reaction as a function of temperature. The symbols show the experimental results: from this work (filled circles, the error bars corresponding to 95% confidence limits); and those of Stevens *et al.*[58] (open triangles, with their quoted uncertainties). The solid and short-dashed blue lines represent the predictions of the scattering calculations of Lique and Alexander, with, respectively, inclusion and exclusion of non-BO coupling. Also shown is the Arrhenius temperature dependence proposed by Persky and Kornweitz[53] (alternating short-long dashed line), the predictions of the single PES quantum scattering calculations of Zhu *et al.*[55,56] (long-dashed line), and the quantum reactive scattering calculations of Aquilanti *et al.*[59,60] (green dashed-dotted line) performed on their PES III. Adapted from Tizniti et al.[54]

calculations were then used to predict the rate constant of $F + H_2$ reaction down to 10 K and below with H_2 in local thermodynamic equilibrium (essentially pure *para*-H_2 at 10 K). The results of these predictions were incorporated in a simple astrochemical model linking H_2 and HF abundances, and it was shown that the new results resulted in an increase up to a factor of 2 in predicted H_2 density (and therefore total mass) in cold diffuse ISCs.[54]

1.3.4 Thermodynamics—The HO_3 Radical

The extremely cold collisional environment associated with uniform supersonic flows has found application not only in reaction kinetics, but also in studies of the thermodynamics of weakly bound species such as PAH (polycyclic aromatic hydrocarbon) clusters[31,61,62] and the $HO\cdots O_2$ or HO_3 radical.[63,64]

The hydroxyl radical (OH) has long been recognized as playing a crucial role in the chemistry of the Earth's atmosphere,[65] as it contributes to the destruction of ozone in the troposphere and initiates oxidation processes in the troposphere. O_2 is known to form chemical bonds with various atoms

(H, F, Cl, *etc.*) and radicals (CH_3 and other alkyl radicals), and it is also suspected to form a weakly bound complex ($HO–O_2$), which could play a significant role in atmospheric chemistry if a sizeable fraction of OH was actually "locked" in these hydroxyl-peroxy radicals. The importance of this temporary reservoir of OH depends on the value of the dissociation energy of the $HO-O_2$ bond (D_0) or, equivalently, on the standard enthalpy of formation of HO_3 ($\Delta_f H^0$). These thermodynamic data can be determined from the equilibrium constant K_c for the reaction $OH + O_2 \rightleftharpoons HO_3$ by using the two following standard thermodynamic equations:

$$K_c = \frac{[HO_3]}{[OH]\,[O_2]} = \frac{q_{HO_3}}{q_{OH}q_{O_2}} \exp\left(D_0/RT\right), \tag{1.13}$$

where $[i]$ is the concentration of component i in the equilibrium mixture, q_i is the partition function for the ith component in unit volume and D_0 is the $HO-O_2$ bond dissociation energy; that is, the difference between the zeroth energy levels of the $OH + O_2$ reactants and the HO_3 product, and

$$K^0 = \exp[(-\Delta_r H^0 + T\Delta_r S^0)/RT], \tag{1.14}$$

where $\Delta_r H^0$ and $\Delta_r S^0$ are the standard changes in enthalpy and entropy associated with the reaction.

Because the partition functions and standard molar entropies for OH, O_2, and HO_3 can be calculated by using known spectroscopic data, determination of the equilibrium constant allows one to calculate $D_0(HO-O_2)$ and ($\Delta_r H^0$), the standard change in enthalpy for the reaction.

In order to estimate K_c, we used a method based on observations of the kinetics behaviour of OH radicals in the presence of O_2. This method has been employed previously for alkyl peroxy ($R-O_2$) radicals[66] and for the $HC-N_2$ species.[67] We examined the kinetics in the small range of temperatures at which [OH] decays to an equilibrium value significantly greater than zero—that is, to an OH concentration at long times, $[OH]_\infty$, of about a half of the concentration at zero time, $[OH]_0$. Because the enthalpy change of the $OH + O_2 \rightarrow HO_3$ reaction is expected to be low, it is necessary to perform experiments at low temperatures.

Under circumstances in which the kinetics of both the forward and reverse reactions must be considered and no other processes contribute to changes in the concentrations of OH and HO_3, the effective first-order rate constant, k_{1st}, associated with the exponential decay of [OH] to an equilibrium level, corresponds to the sum of the pseudo-first-order rate constants for the forward and reverse reactions:

$$k_{1st} = k_f + k_r = k_{3rd,ass}\ [O_2][M] + k_{2nd,diss}[M], \tag{1.15}$$

where [M] is the total gas density and $k_{3rd,ass}$ and $k_{2nd,diss}$ are the third-order rate constant for association of $OH + O_2$ and the second-order rate constant for dissociation of HO_3, respectively. The equilibrium constant, $K_c = k_{\mathrm{3rd,ass}}/k_{\mathrm{2nd,diss}}$, can be written as

$$K_\mathrm{c} = \frac{[\mathrm{HO_3}]_\infty}{[\mathrm{OH}]_\infty\,[\mathrm{O_2}]} = \frac{[\mathrm{OH}]_\infty - [\mathrm{OH}]_0}{[\mathrm{OH}]_\infty\,[\mathrm{O_2}]} = \frac{1 - \left\{[\mathrm{OH}]_\infty/[\mathrm{OH}]_0\right\}}{[\mathrm{O_2}]\left\{[\mathrm{OH}]_\infty/[\mathrm{OH}]_0\right\}}. \tag{1.16}$$

To access suitably low temperatures, which we found to be in the 85 − 105 K range, we have employed the CRESU method. A Laval nozzle was designed specifically for performing experiments on the OH + O_2 reaction in this temperature range, which produced a total density in the gas flow between 4×10^{17} and 6×10^{17} molecule cm^{-3}. The temperature was tuned either by seeding the O_2 in the flow with different concentrations of argon and adjusting as necessary the pressure in the reservoir upstream from the nozzle or (over a smaller range) by varying the pressure in the main chamber. OH radicals were generated by PLP of H_2O_2 using the output from an excimer laser at 248 nm, and subsequent changes in their concentration were followed by using a frequency-doubled tuneable dye laser to generate LIF signals, as the time delay between the photolysis laser and the probe laser was varied. The variation of OH concentration in the present experiments where, at zero time, the concentration of OH is $[\mathrm{OH}]_0$ and the concentration of HO_3 is zero, is then given by:

$$[\mathrm{OH}]_t = [\mathrm{OH}]_0 \left\{ \frac{k_{\mathrm{2nd,diss}}}{k_{\mathrm{3rd,ass}}\,[\mathrm{O_2}] + k_{\mathrm{2nd,diss}}} + \frac{k_{\mathrm{3rd,ass}}\,[\mathrm{O_2}]}{k_{\mathrm{3rd,ass}}\,[\mathrm{O_2}] + k_{\mathrm{2nd,diss}}} \exp\left(-k_{\mathrm{1st}}t\right) \right\}. \tag{1.17}$$

Determining the magnitude of the second term on the right-hand-side of this equation allows finding $k^0_{\mathrm{3rd,ass}}\,[O_2]\big/k^0_{\mathrm{2nd,diss}}$; that is, the product of the equilibrium constant for the reaction, $K_\mathrm{c} = k^0_{\mathrm{3rd,ass}}\big/k^0_{\mathrm{2nd,diss}}$, and $[\mathrm{O_2}]$. To take into account loss of OH radicals from the region illuminated by the probe laser by diffusion, we also included a slow background first-order loss decay, k^0_{1st}, in the kinetic equation for the OH radical:

$$\begin{aligned}[\mathrm{OH}]_t &= [\mathrm{OH}]_0 \exp(-k^0_{\mathrm{1st}}t) \\ &\quad \left\{ \frac{k_{\mathrm{2nd,diss}}}{k_{\mathrm{3rd,ass}}\,[\mathrm{O_2}] + k_{\mathrm{2nd,diss}}} + \frac{k_{\mathrm{3rd,ass}}\,[\mathrm{O_2}]}{k_{\mathrm{3rd,ass}}\,[\mathrm{O_2}] + k_{\mathrm{2nd,diss}}} \exp\left(-k_{\mathrm{1st}}t\right) \right\}.\end{aligned} \tag{1.18}$$

The traces of LIF signals *versus* time recorded were analyzed by first evaluating k^0_{1st} from a single exponential fit to the LIF signals recorded in the experiment replacing O_2 by N_2 and then by fitting the signals in the trace in which O_2 was present to a function of the form $\exp(-k^0_{\mathrm{1st}}t)\,\{A + B\exp\left(-k_{\mathrm{1st}}t\right)\}$. The parameters $\boldsymbol{A}$ and $(A + B)$ that are derived are proportional to $[\mathrm{OH}]_\infty$ and $[\mathrm{OH}]_0$, and the ratio $A/(A + B)$ corresponds to the value of $[\mathrm{OH}]_\infty/[\mathrm{OH}]_0$ required to calculate the equilibrium constant K_c. An example of a fit to experimental data is shown in Figure 1.13. This procedure was performed at seven temperatures between 87.4 K and 99.8 K. Having obtained values of K_c, we calculated values of the

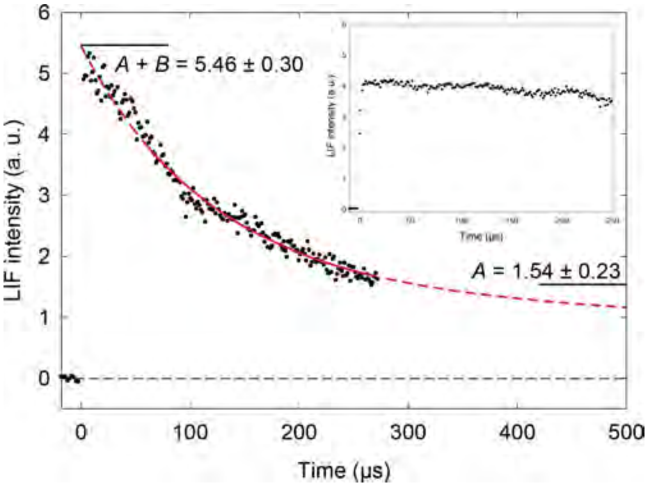

Figure 1.13 LIF signals from OH recorded in a CRESU experiment with $T = 95.4$ K, $[O_2] = 4.9 \times 10^{17}$ molecule cm^{-3}, $[M] = 6.1 \times 10^{17}$ molecule cm^{-3}. The signals are fitted to a function of the form $\exp(-k^0_{1st})[A + B\exp(-k_{1st}t)]$. Values of $(A + B)$ and A, derived from the fitting, are shown on the axes. The insert shows the variation of LIF signals with time from a similar experiment with N_2 present in place of O_2.[64] From S. D. Le Picard, M. Tizniti, A. Canosa, I. R. Sims and I. W. M. Smith, *Science*, 2010, **328**, 1258-1262, https://doi.org/10.1103/PhysRevLett.116.113401. Reprinted with permission from AAAS.

bond dissociation energy, D_0, using the partition functions for HO_3, OH, and O_2, which we estimated using spectroscopic data and standard formulas. Values of D_0 obtained from each of the experiments performed at temperatures between 87.4 K and 99.8 K were averaged to give a mean value of (12.3 ±0.3) kJ mol^{-1}. Calculating $\Delta_r S^0$ using the spectroscopic properties (rovibronic levels, rotational constants, vibrational frequencies, …) of HO_3, O_2 and OH as well as the formulas relating partition functions to standard entropies, we determined an enthalpy change $\Delta_r H^0$ at 298 K for the reaction $OH + O_2 \rightarrow HO_3$ of $-(17.9 \pm 0.3)$ kJ mol^{-1}.

The value of D_0 determined in our experiments suggests that the fraction of OH bound to O_2 is less than 0.1% at all altitudes in the Earth's atmosphere. Consequently, the formation of HO_3 through the association of OH radicals with O_2 plays no meaningful role in the chemistry of Earth's atmosphere.

1.3.5 Kinetics of Cluster Formation: Water Clusters $(H_2O)_n$

The rates and mechanisms by which individual molecules in a supersaturated gas coalesce to form the first oligomers and eventually liquid droplets are both important and still poorly understood. Although nucleation processes have been intensively studied (see Kathmann[68] and references therein) because they find applications in a large variety of scientific fields, major uncertainties remain in our understanding of the mechanisms for particle formation. Numerous experimental methods (see Zhang *et al.*[69] and references therein) have been developed for estimating nucleation rates, *i.e.* the number of nuclei formed per unit time and per unit volume, as a function of saturation and temperature. These rates vary over orders of magnitude and are very sensitive to the physical conditions, such as the temperature of the environment or the concentrations and the nature of the species involved in the clustering process. Classical nucleation theory, however, usually fails to provide accurate estimates of the absolute nucleation rates.[70,71] Understanding of the first steps of nucleation mechanisms can also be approached through a dynamical treatment where gas-phase association and dissociation rate coefficients are considered. From a theoretical point of view, this approach requires an accurate description of the intermolecular potential, the reaction rates being very sensitive to the details of the molecular interactions. From an experimental point of view, it is essential to perform experiments under very well-controlled physical conditions.

CRESU supersonic flows where the expanded gas is under supersaturated conditions at a well-defined temperature and density possess in addition uniform velocities, which enables an accurate correlation of distance to reaction time, operating in flow-tube mode. They are therefore well suited to observe the temporal evolution of the first step of molecular cluster formation. In addition, at the lowest temperatures reached in the CRESU flows, the dissociation rates can be so small that evaporation is negligible, which greatly simplifies the analysis of the growth of the clusters. The kinetics then corresponds to a barrierless process that is governed by the kinetics of collisions, with dimer formation being the critical step. Finally, because the very low temperatures are accessed under supersaturation conditions, the first step of homogeneous nucleation processes can be observed even for molecules forming van der Waals complexes with binding energies of a few kJ mol^{-1}.

Using this flow-tube mode, we have studied the dimerization of benzene,[72] as well as several PAHs, notably pyrene[31,62] and anthracene,[61] in relation to the early stages of soot formation[31] as well as for application to planetary atmospheres[61] and circumstellar shells.[62] Recently, we reported a combined experimental and theoretical kinetics study of neutral water cluster formation at low temperature.[30] The experiments were performed using cold uniform supersonic flows of helium generated by a series of Laval nozzles in which a small ($<1\%$) and controlled amount of water vapour was introduced. The observed kinetics of formation of water clusters was fitted using a model in which theoretical predictions of the rate coefficients for the first steps of clustering were incorporated. The time evolution of the neutral monomers, as well as clusters formed due to the low temperature of the environment, were monitored using an electron impact ionization time-of-flight mass spectrometry technique after skimming out the centre of the flows at various distances from the Laval nozzle exits (see Figure 1.14). Greater

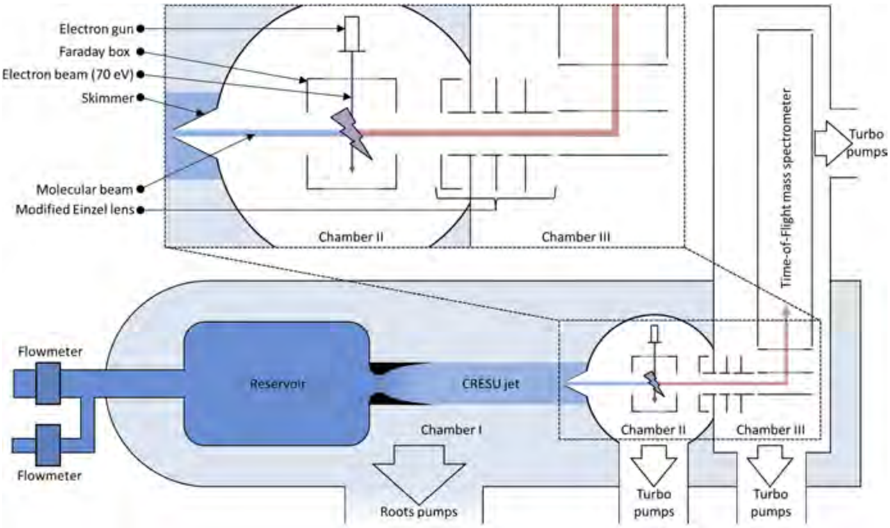

Figure 1.14 Experimental setup combining the CRESU supersonic flows with electron impact ionization/time-of-flight mass spectrometry: the CRESU jet is generated by supersonic expansion from the reservoir to the chamber I through a Laval nozzle. The centre of the flow is then skimmed to generate a molecular beam in chamber II where the gas is ionized by an electron beam. Ions formed are then driven into a time-of-flight mass spectrometer in chamber III. Reprinted figure with permission from J. Bourgalais, V. Roussel, M. Capron, A. Benidar, A. W. Jasper, S. J. Klippenstein, L. Biennier and S. D. Le Picard, *Phys. Rev. Lett.*, **116**, 5, 113401, 2016, https://doi.org/10.1103/PhysRevLett.116.113401.[30] Copyright 2016 by the American Physical Society.

distances correspond to longer cluster formation times within the supersonic flow. The water vapour was introduced into the CRESU reservoir through a controlled evaporation mixing system to ensure the homogeneity of the injected gases. This also allowed an absolute calibration of the monomer ion signal.

By varying the distance between the exit of the Laval nozzles and the skimmer, the time evolution of the ion water monomer and cluster signals were determined for various initial water concentrations at temperatures between 23 K and 69 K. Because the ionization cross-section and the transmission of the experimental setup is not readily accessible, we assumed that for water clusters, the integrated ion signals $I_n(t)$ were related through the expression

$$I_n\,(t) = \gamma_{n+2}\left[(\mathrm{H_2O})_{n+2}\right](t)\,, \tag{1.19}$$

where γ_{n+2} is a size-dependent proportionality factor. Figure 1.15 shows the time evolution on a relative scale of neutral water clusters (n being the number of water molecules in the cluster) derived from the integrated ion signals for various cluster sizes at 35.9 K.

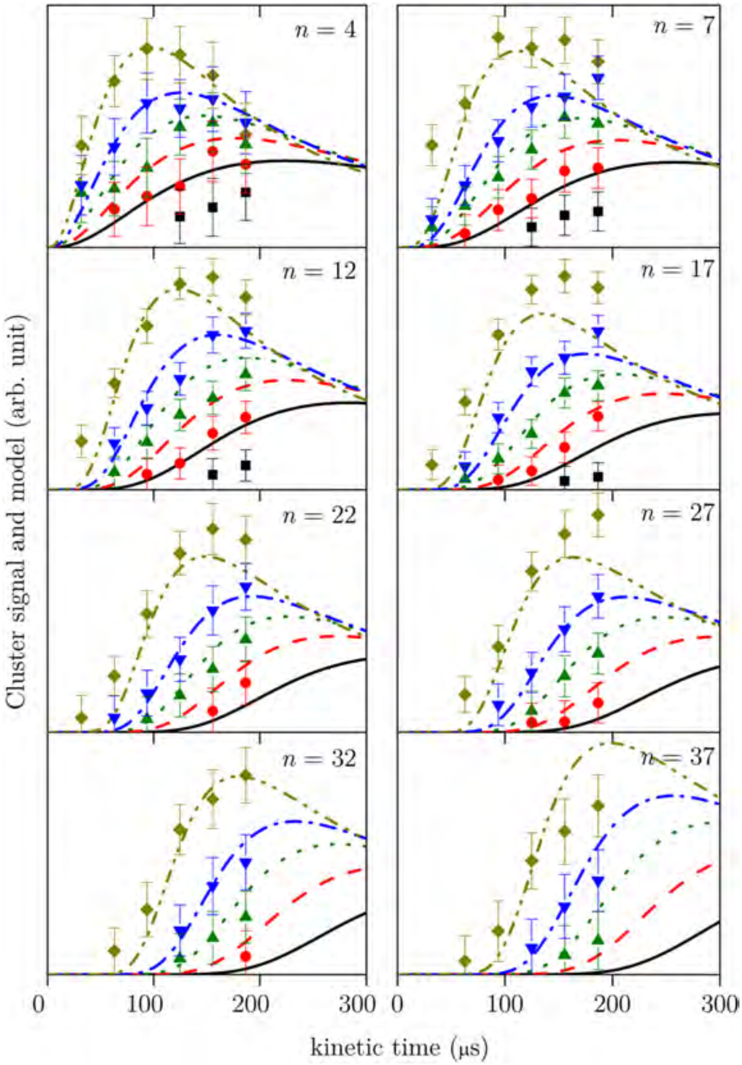

Figure 1.15 Time evolution of $(H_2O)_n$ clusters at 35.9 K for water monomer densities introduced in the CRESU flows of 1.22×10^{14} cm^{-3} (black squares and black solid lines); 1.54×10^{14} cm^{-3} (red circles and red dashed lines); 1.85×10^{14} cm^{-3} (dark green triangles and dark green dotted lines); 2.17×10^{14} cm^{-3} (blue downward triangles and blue dot-dashed lines); 2.79×10^{14} cm^{-3} (light green lozenges and light green dot-dot-dashed lines). Lines refer to the kinetic model with calculated rate constants. Reprinted figure with permission from J. Bourgalais, V. Roussel, M. Capron, A. Benidar, A. W. Jasper, S. J. Klippenstein, L. Biennier and S. D. Le Picard, *Phys. Rev. Lett.*, **116**, 5, 113401, 2016, https://doi.org/10.1103/PhysRevLett.116.113401.[30] Copyright 2016 by the American Physical Society.

The formation of water clusters can be treated in terms of bimolecular formation of energized clusters, which can then either be stabilized by collision with a third body (helium in this case) or redissociate. In the framework of Rice–Ramsperger–Kasse–Marcus theory,[73] the dimer formation from two monomers for instance, can be expressed as follows:

$$H_2O + H_2O \rightleftharpoons (H_2O)_2{}^* \overset{k_{He}[He]}{\rightarrow} (H_2O)_2, \qquad (1.20)$$

where the energized complex $(H_2O)_2{}^*$ formed with a rate coefficient k_{assoc}, can either dissociate with a rate coefficient k_{dissoc} or be deactivated with a third-order rate coefficient k_{He} by collisions with the helium buffer gas.

To extract quantitative information from the time evolution of the water cluster populations observed in the CRESU flows, a kinetic model based on theoretical calculations has been developed. In this model we assumed that the merging of two clusters or of a cluster and a monomer can form a cluster of n molecules and that any cluster loss is due to reaction with another cluster or a monomer. Theoretical predictions show that dissociation from the clusters can be ignored due to the low temperatures of the present experiments. For the association between $(H_2O)_i$ and $(H_2O)_j$ with i and j both greater than unity, the evaporation of a monomer from the initially formed adduct is significantly exothermic. As a result, at least for the specific systems examined theoretically, such association processes lead to the evaporation of a monomer with a rate coefficient equal to the high-pressure association rate. The stabilization rate is considered to be effectively zero for the size of clusters of the present study.

Coupling *ab initio* transition state theory to evaluate the microcanonical dissociation rate coefficients $k_{dissoc}(E)$, with simple models for estimating the energy transfer rates to obtain a master equation for the time dependence of the energy-resolved state populations, the temperature- and pressure-dependent association rate coefficients $k_{ass(i,j)}(T, P)$ were predicted for $(i, j) = (1,1), (1,2), (1,3), (1,4), (1,5), (2,2), (2,3), (2,4), \text{and} (3,3)$. For this purpose potential energy values for the interaction between rigid reactants at arbitrary separations and orientations were obtained *via* direct *ab initio* evaluations. Figure 1.16 displays the predicted pressure dependence of the rate coefficients for the $(H_2O) + (H_2O)$ and $(H_2O) + (H_2O)_2$ reactions for the temperatures of the experimental study. It can be seen that the $k_{ass(1,2)}$ (dashed lines) rate coefficient approaches its high-pressure limit at much lower pressures than does $k_{ass(1,1)}$ (solid lines). This is due to the increase in the number of low-frequency modes, which yields a decrease in the rate of dissociation at a given energy, and thus an increase in the probability of collisional stabilization at a given pressure. A similar shift toward the high-pressure limit was found for larger systems.

The experimental data were then fitted using the kinetic model described above, incorporating the predicted rate coefficients. For each temperature, values of $k_{ass(i,j)}$ for larger i and j were supposed equal to a single rate coefficient k_∞ that was used as a fitting parameter. These k_∞ values were found to

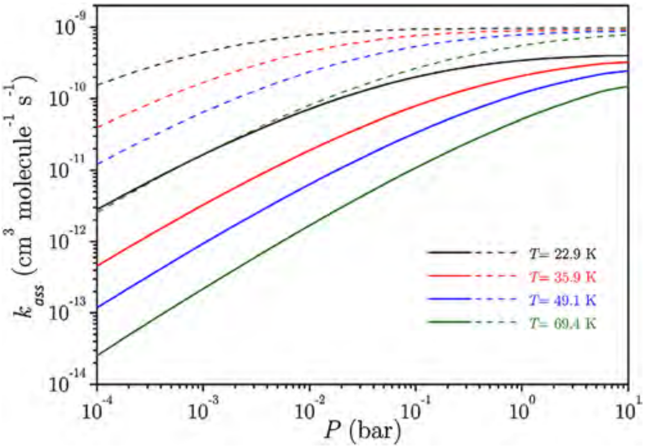

Figure 1.16 Theoretically predicted temperature- and pressure-dependent association rate coefficients k_{ass} for H_2O + H_2O (solid lines) and H_2O + $(H_2O)_2$ (dashed lines). The experimentally studied pressure range is from about 10^{-3} to 10^{-4} bar. Reprinted figure with permission from J. Bourgalais, V. Roussel, M. Capron, A. Benidar, A. W. Jasper, S. J. Klippenstein, L. Biennier and S. D. Le Picard, *Phys. Rev. Lett.*, **116**, 5, 113401, 2016, https://doi.org/10.1103/PhysRevLett.116.113401.[30] Copyright 2016 by the American Physical Society.

be reasonably consistent with the calculated high-pressure values for smaller clusters. Figure 1.15 shows the comparison between the experimental data (symbols) and the kinetic model (dashed and solid lines) at 35.9 K, for five different initial water densities in the case of neutral clusters composed of 4–37 monomers. To compare the time evolution given by the model with the experimental data, the population of clusters given by the model was arbitrarily normalized to one of the experimental points. Similar results were obtained at 22.9 K, 49.1 K, and 69.4 K.

This combined experimental and theoretical study[30] provides for the first time quantitative information on the rates of the elementary reactions involved in the first steps of water nucleation of over a wide range of physical conditions, as calculations were extended over a larger range of temperatures (20 K to 100 K) and pressures (10^{-6} bar to 10 bar). This work confirms the strong dependence on temperature and pressure of the nucleation process and demonstrates that at low temperature, where cluster dissociation is negligible, their growth is controlled by the kinetics of water dimer formation. It is worth noting that the predicted pressure-dependent fall-off for the dimer formation rate coefficient, $k_{1,1}$, is even more significant at higher temperature and is also important in the reverse dimer dissociation.

Finally, it is interesting to compare the present approach with the classical nucleation models, which focus on the growth and decay of different sized clusters *via* the association and dissociation of monomers. Within the classical model, the steady state nucleation rate, J_{ss} can be written as[74]

$$J_{ss} = k_{\mathrm{ass},1}\,[\mathrm{H_2O}]\left(1 + \frac{k_{\mathrm{diss},2}}{k_{\mathrm{ass},2}} + \frac{k_{\mathrm{diss},3}k_{\mathrm{diss},2}}{k_{\mathrm{ass},3}k_{\mathrm{ass},2}} + \frac{k_{\mathrm{diss},4}k_{\mathrm{diss},3}k_{\mathrm{diss},2}}{k_{\mathrm{ass},4}k_{\mathrm{ass},3}k_{\mathrm{ass},2}} + \ldots\right)^{-1}, \tag{1.21}$$

where the $k_{\mathrm{ass},i}$ quantities are the association rates for the addition of a monomer to a cluster of size i, and the $k_{\mathrm{diss},i}$ terms are the dissociation rates for the loss of a monomer from a cluster of size i. The presence of the ratio of rates in this expression leads to a dependence on the thermodynamics of the monomer addition processes rather than their kinetics. As soon as the critical cluster size (where $k_{\mathrm{diss},i} = k_{\mathrm{ass},i} = 1$) is reached, the association rate for larger clusters exceeds the dissociation rate and growth is unbounded. At the low temperatures and pressures of the present experiments the various $k_{\mathrm{diss},i}$ coefficients were found to be several orders of magnitude smaller than the $k_{\mathrm{ass},i}$ rate coefficients and the nucleation rate, J_{SS}, reduces to $k_{\mathrm{ass},i}$ $[\mathrm{H_2O}]$. This means that the critical cluster size is 2, and $k_{\mathrm{ass},i}$ is the central parameter determining the rate of growth of clusters (*i.e.* the nucleation rate) in the present experiments. In such conditions, the growth of the clusters is kinetically controlled rather than thermodynamically controlled, as there are no reverse processes to bring about equilibration.

This study opens the way to further investigation of the kinetics of homogeneous nucleation of small molecular species. Such kinetics studies will provide valuable information on low-temperature energy transfers, collision rates, and binding energies of van der Waals bound molecules. Beyond fundamental aspects, low-temperature kinetics of molecular cluster formation will be of interest for the exploration of the condensation processes in cold planetary atmospheres.

1.3.6 Product Branching Studies at Low Temperatures—C_2H + Butenes

The study of the kinetics of C_2H reactions for astrochemical interest began very early, since it was one of the first species detected in the interstellar medium as early as 1974,[75] on Titan in 1991,[76] and more recently in star formation regions.[77] Following this interest, numerous studies of the reactivity of C_2H and the products of these reactions have been carried out.[78]

This section presents a set of experiments[79] that were performed on the 'Laval machine', a pulsed Laval nozzle system in use at the Advanced Light Source synchrotron (Berkeley, USA).[80] This experimental setup samples the uniform flow through a pinhole in an airfoil, followed by synchrotron VUV ionization, and quadrupole mass discrimination. The main advantage of this setup is the low gas consumption (compared to continuous CRESU) and the very high resolution in product discrimination. The study did not evaluate a temperature change effect, and was focused on the study of C_2H radical colliding with butene (C_4H_8) isomers: 1-butene, 2-butene (*cis* and *trans*), and isobutene (2-methylpropene) and reaction products, at 79 K. The reaction C_2H + 1-butene is treated here as example. The process does not differ for other reactions in the study.

In the setup, C_2H is produced by PLP of acetylene (C_2H_2) at 193 nm. It is injected along with 1-butene and nitrogen as carrier gas. The nozzle expansion produced a pulsed beam at 79 K rich in C_2H_2, yielding C_2H after the laser pulse. C_2H starts to react with C_2H_2, 1-butene, and possible photofragments of 1-butene. It is then necessary to determine whether or not a species is a reaction product or photofragment.

First, a mass spectrum at high ionization energy is obtained with only 1-butene in the flow, to study its fragments. This is the spectrum *A* in Figure 1.17. Products of dissociation were identical to previous work.[81]

A spectrum with all species in the flow is then obtained (*B*), and (*A*) is used as a baseline to compute (*C*), showing products. On signals (*B*) and (*C*), the peak at mass 50 a.m.u. is diacetylene, from the recombination of C_2H with C_2H_2.[82] The second part of the study is to determine what are the species corresponding to these mass channels. In the case of 1-butene + C_2H, mass channels 52 and 66 are populated by products of the reaction. By scanning the mass channel against the ionization energy, which is the major advantage of using a tuneable VUV source such as a synchrotron, it is possible to fit signals against ionization curve of pure products beforehand. Figure 1.18 shows the result of this ionization scan. In the case of C_2H + 1-butene, in each of these channels, products are obtained pure, but it is frequent that two or more products are found, and a fit must be done to find the adequate fractions of products in that specific mass channel. The branching ratio, it is simply the ratio of ion counts at high energy for every product,

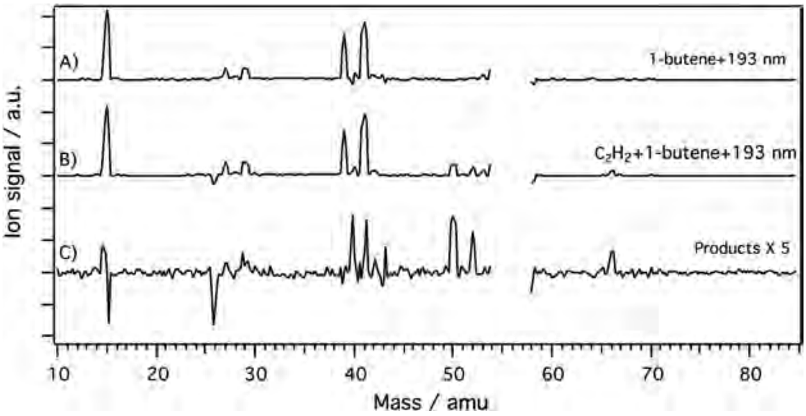

Figure 1.17 Product mass spectra. A: 1-butene photofragments. B: all reaction species (reagents and products). C: 5 × (B − A), showing only reaction products. Reprinted with permission from ref. 79. Copyright 2013 American Chemical Society.

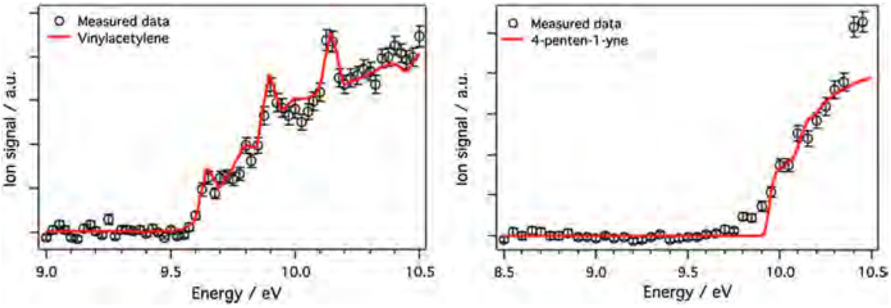

Figure 1.18 Left: ion signal on mass channel 52 with increasing ionization energy, shown with the photoionization spectrum for vinylacetylene (but-1-en-3-yne). Right: ion signal on mass channel 66 with increasing ionization energy, shown with the photoionization spectrum for 4-penten-1-yne. Reprinted with permission from ref. 79. Copyright 2013 American Chemical Society.

compared to the sum of all ion counts across all channels. This gives for this reaction a fraction of (65 ± 10)% for vinylacetylene and (35 ± 10)% for 4-penten-1-yne.

The last part of the study is the determination of the reaction rate. For this experiment the quadrupole mass spectrometer is kept at a single mass, looking at the time dependence of the ion signal, also keeping the ionization energy constant. The time-dependent ion signal at a particular mass to charge ratio, if it corresponds to a primary reaction product, will obey a function $C(t) = A\{1 - \exp(-k_{1st}t)\}$, with k_{1st} the pseudo-first-order reaction rate constant to be determined. In reality, the function is modified because of the normal distribution of ions at the arrival time in the quadrupole, and the resulting function is a convolution of the exponential with a Gaussian. Nonetheless, it is possible to deconvolute the resulting signal back to the original exponential function to obtain the rate constant for that density of 1-butene. By repeating the experiment for densities of 1-butene, the second order rate constant for C_2H + 1-butene at that specific temperature is obtained. It is the slope of the function $k_{1st}(d) = k_{2nd}d + k_0$, where d is the reagent density. The rate constant measured for that reaction was $(1.9 \pm 0.5) \times 10^{-10}$ cm^3 molecule^{-1} s^{-1}.

1.3.7 Product Branching Studies at Low Temperatures—The CPUF Technique

The most sensitive and widely used detection methods in the gas-phase (*e.g.* LIF, mass spectrometry), while well adapted for determining overall rate constants, face serious challenges in correlating signal intensities to actual concentrations of multiple reaction products. Furthermore, these methods rarely provide detailed structural information. Rotational spectroscopy, on the other hand, is highly specific, giving unambiguous identification of each chemical species present (provided it possesses at least a modest permanent electric dipole, which is the case for the vast majority of molecules—this is the overall selection rule for rotational transitions). But traditionally it suffers from a number of drawbacks, which have severely restricted its wider use in applications such as chemical kinetics and reaction dynamics. The sensitivity of direct microwave and millimetre-wave detection schemes had been judged to be inferior to laser-based schemes. And the need to tune the resonant cavities coupled to the extremely high resolution of modern microwave instruments means that scanning between rotational lines belonging to different species can be very slow.

The advent of the Chirped Pulse Fourier-Transform MicroWave (CP-FTMW) technique,[83] invented by Brooks Pate and co-workers at the University of Virginia, has completely turned the tables, and provoked a revolution in the spectroscopic world, projecting rotational spectroscopy to the forefront of applications across a wide range of fields. Advances in high-speed digital electronics have enabled this new technique:[84] a high-bandwidth, frequency-stabilized arbitrary waveform generator is used to produce a short microwave pulse (*ca.* 1 μs or less) with a frequency sweep that is linear in time.[83] This chirped pulse is up-converted to the frequency range of interest and, if necessary, amplified for irradiation of the sample. The molecular sample absorbs at all rotational transitions within the frequency range of the chirp and is polarized by the radiation. Free induction decay (FID) of the polarization ensues and the emitted FID radiation is collected, down-converted, and averaged in the time domain by a high-bandwidth oscilloscope, after which the collected signal is Fourier-transformed to give the rotational spectrum at MHz resolution. The use of the chirped pulse as opposed to the traditional approach of narrowband shot-by-shot scanning of the microwave frequency in a resonant cavity has led to an improvement by several orders of magnitude in the rate of data acquisition, as the power delivered to the sample is decoupled from the bandwidth, and dead time associated with stepping the cavity resonance frequency is eliminated.[83,85] Furthermore, by covering a wide range of frequencies in a single pulse, this technique enables simultaneous detection of multiple species.

In order to achieve the strongest signals, CP-FTMW spectra are typically recorded for cold samples to maximize the population difference between adjacent rotational levels, and pulsed free jet expansions have usually been used. However, there are numerous disadvantages associated with the use of free jet expansions for this purpose: they are non-equilibrium environments in which the temperature varies strongly along the beam for the first several nozzle diameters, and the density varies throughout the expansion; reactive processes and photochemical systems cannot be cooled and thermalized in any consistent or reliable way; and the total number of sample molecules in the irradiated volume is limited, constraining the maximum signal levels.

An alternative approach is to employ the very cold, thermalized environment provided by uniform supersonic expansions employed in the

CRESU technique. In a recent development the CP-FTMW method has been combined with a pulsed version of the CRESU technique, in a combination referred to as CPUF (Chirped Pulse in Uniform Flow).[24] This new method (see Figure 1.19) provides broadband spectra with MHz resolution and allows monitoring, on the μs timescale, of the appearance of transient reaction products. Such products are often born at very low concentrations and very hot, and would be impossible to detect without the drastic enhancement in sensitivity afforded by the generation of large volumes of (translationally and) rotationally cooled products afforded by the use of the CRESU technique.

In essence, CPUF exploits the extremely cold, collisional environment of CRESU flows to rotationally cool the hot photo- or reaction products (resulting from exothermic reactions) to collapse their rotational state distributions to much lower values of rotational energy. This results, at least for small to medium-sized polyatomic molecules, in a drastic increase in difference in adjacent rotational level populations, and a shift of the maximum intensity of their rotational spectra to below 100 GHz, into the region accessible by modern CPMW spectrometers, exploiting the

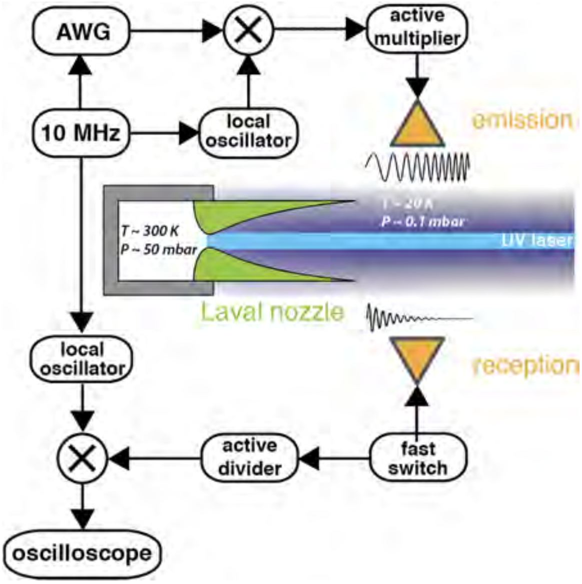

Figure 1.19 A schematic diagram of the CPUF technique. A chirped pulse is generated in an arbitrary waveform generator (AWG), locked to a 10 MHz Rb oscillator. The chirped pulse is up-converted to the required frequency range, amplified if necessary, and broadcast into the CRESU flow. A UV photolysis laser creates radicals within the flow, and these react with added co-reagent. Dipolar product molecules are polarized and their subsequent free induction decay is captured, frequency down-converted and recorded by a broadband oscilloscope. Fourier transformation of this signal yields the rotational spectrum.

frequency agility of new arbitrary waveform generators *via* segmented chirp techniques.[86]

Very recently, the CPUF technique was used to determine product branching ratios for the first time in a multichannel reaction between CN radicals and propyne (C_3H_4).[87] This reaction can proceed by direct abstraction:

$$\mathrm{CN} + \mathrm{CH_3CCH} \rightarrow \mathrm{HCN} + \mathrm{CH_2CCH}, \tag{1.22}$$

by addition followed by methyl elimination:

$$\mathrm{CN} + \mathrm{CH_3CCH} \rightarrow \mathrm{CH_3} + \mathrm{HCCCN}, \tag{1.23}$$

or by addition followed by H elimination:

$$\mathrm{CN} + \mathrm{CH_3CCH} \rightarrow \mathrm{H} + \mathrm{CH_3CCCN} \tag{1.24}$$

$$\mathrm{CN} + \mathrm{CH_3CCH} \rightarrow \mathrm{H} + \mathrm{CH_2CCHCN}. \tag{1.25}$$

Using a chirped pulse in the 60–90 GHz frequency region, quantitative branching ratios were established for all products as 12(5)%, 66(4)%, 22(6)%, and 0(8)% into HCN, HCCCN, CH_3CCCN, and CH_2CCHCN, respectively. The values were consistent with statistical calculations based on new *ab initio* results at the CBS-QB3 level of theory, a composite "complete basis set" method developed by Petersson and co-workers.[88,89] A previous determination of the products of this reaction, using the crossed molecular beam technique at higher energies,[90,91] found somewhat different product branching ratios. This previous work may have suffered from kinematic constraints that favour detection of products with small centre-of-mass recoil velocities. As such, these studies were unable to detect the CH_3 elimination product, HCCCN, or the direct reaction to HCN.

1.4 Conclusion and Perspectives

The CRESU technique was born in an aerodynamics laboratory, equipped with the enormous pumping capacity necessary to generate the necessary flows for a hypersonic wind tunnel. The brainchild of Bertrand Rowe and colleagues, it was initially only applied to ion–molecule reaction kinetics, perhaps because these were the only bimolecular reactions thought to remain fast at very low temperatures. A revolution in the applicability of the CRESU technique came with its combination with laser photochemical kinetics techniques for the study of neutral–neutral reactions, coupled with the construction of two dedicated CRESU facilities in Rennes and Birmingham in the early to mid-1990s, requiring somewhat more modest, though still impressive, pumping capacities. Since that time, the technique has been applied to the study of a wide range of chemical reactions, cluster formation and energy transfer processes, some of which have been detailed in this chapter. Significant further developments of the technique in Rennes have included:

- the coupling of the CRESU with pulsed tuneable infrared and/or vacuum ultraviolet lasers for the study of vibrational and rotational energy transfer[92,93] and atom–radical reactions[36]
- the development of mass-spectrometric sampling of the CRESU flow to study clustering reactions[30,31]
- the design and application of Laval nozzles where the buffer gas is also the reactant (either entirely or at a large fraction of the total), enabling the study of relatively slow processes dominated by tunnelling,[54] or relaxation processes to yield thermochemical information[64]

The unique environment of uniform supersonic flows continues to be attractive for new applications in physical chemistry, molecular physics and experimental astrochemistry. Current and future developments in Rennes include:

- the exploitation of hydrogen supersonic flows coupled with IR(V)UVDR techniques to study rotational energy transfer in collisions of astrochemically important small molecules and radicals in collision with H_2, the commonest molecule in space
- the combination of a pulsed CRESU apparatus using fast piezoelectric valves with synchrotron photoionization mass spectrometry based on photoelectron–photoion coincidence techniques to provide much-needed data on the product branching ratios of low-temperature reactions
- the implementation of the new CPUF technique[87,94] in the high-quality continuous supersonic flows available in Rennes to further increase its sensitivity and apply it to a wide range of problems in low-temperature chemical kinetics

Acknowledgements

The authors acknowledge the invaluable contributions of many colleagues at Rennes and elsewhere to the development of the CRESU technique, notably Bertrand Rowe and Ian W. M. Smith. We would also like to thank in particular the many young researchers (PhD students and postdocs) and the technical and mechanical workshop staff who have played an essential role in all the work described in this chapter. We are also grateful to the many different agencies that have funded this work over the years, including, notably, in France the CNRS (Centre National de la Recherche Scientifique), especially *via* its multidisciplinary programmes PCMI (Physique et Chimie du Milieu Interstellaire) and PNP (Programme National de Planétologie), and the University of Rennes 1, as well as the ANR (Agence Nationale de la Recherche). In the UK we acknowledge in particular the EPSRC (Engineering and Physical Sciences Research Council) and the University of Birmingham. The collaborative project that led to the development of the CRESU technique as a powerful tool for the study of neutral reaction kinetics would not have been possible without strong support from the European Union's various collaborative research programmes, for which we are particularly grateful.

References

1. I. W. M. Smith, in *Reaction Rate Constant Computations: Theories and Applications*, The Royal Society of Chemistry, 2013, pp. 1–33.
2. I. W. M. Smith, *Chem. Soc. Rev.*, 2008, **37**, 812–826.
3. F. M. Flasar, R. K. Achterberg, B. J. Conrath, P. J. Gierasch, V. G. Kunde, C. A. Nixon, G. L. Bjoraker, D. E. Jennings, P. N. Romani, A. A. Simon-Miller, B. Bezard, A. Coustenis, P. G. J. Irwin, N. A. Teanby, J. Brasunas, J. C. Pearl, M. E. Segura, R. C. Carlson, A. Mamoutkine, P. J. Schinder, A. Barucci, R. Courtin, T. Fouchet, D. Gautier, E. Lellouch, A. Marten, R. Prange, S. Vinatier, D. F. Strobel, S. B. Calcutt, P. L. Read, F. W. Taylor, N. Bowles, R. E. Samuelson, G. S. Orton, L. J. Spilker, T. C. Owen, J. R. Spencer, M. R. Showalter, C. Ferrari, M. M. Abbas, F. Raulin, S. Edgington, P. Ade and E. H. Wishnow, *Science*, 2005, **308**, 975–978.
4. M. Agundez and V. Wakelam, *Chem. Rev.*, 2013, **113**, 8710–8737.
5. E. Herbst, *J. Phys. Chem. A*, 2005, **109**, 4017–4029.
6. G. Dupeyrat, J. B. Marquette and B. R. Rowe, *Phys. Fluids*, 1985, **28**, 1273–1279.
7. B. R. Rowe, G. Dupeyrat, J. B. Marquette and P. Gaucherel, *J. Chem. Phys.*, 1984, **80**, 4915–4921.
8. I. R. Sims, J. L. Queffelec, A. Defrance, C. Rebrion-Rowe, D. Travers, P. Bocherel, B. R. Rowe and I. W. M. Smith, *J. Chem. Phys.*, 1994, **100**, 4229–4241.
9. P. L. Houston, in *Chemical Kinetics and Reaction Dynamics*, Dover Publications, United States, 2006, p. 114.
10. I. R. Sims, J. L. Queffelec, D. Travers, B. R. Rowe, L. B. Herbert, J. Karthäuser and I. W. M. Smith, *Chem. Phys. Lett.*, 1993, **211**, 461–468.
11. I. R. Sims and I. W. M. Smith, *Annu. Rev. Phys. Chem.*, 1995, **46**, 109–137.
12. Y. Georgievskii and S. J. Klippenstein, *J. Phys. Chem. A*, 2007, **111**, 3802–3811.
13. I. R. Sims and I. W. M. Smith, *Chem. Phys. Lett.*, 1988, **151**, 481–484.
14. D. R. Willey, R. L. Crownover, D. N. Bittner and F. O. Delucia, *J. Chem. Phys.*, 1988, **89**, 1923–1928.
15. T. M. Goyette, F. C. Delucia and D. R. Willey, *J. Geophys. Res., Planet.*, 1991, **96**, 17455–17461.
16. J. M. Doyle, B. Friedrich, J. Kim and D. Patterson, *Phys. Rev. A*, 1995, **52**, R2515–R2518.
17. I. R. Sims and I. W. M. Smith, *Chem. Phys. Lett.*, 1988, **151**, 481–484.
18. F. Luo, G. C. McBane, G. S. Kim, C. F. Giese and W. R. Gentry, *J. Chem. Phys.*, 1993, **98**, 3564–3567.
19. N. Balucani, G. Capozza, F. Leonori, E. Segoloni and P. Casavecchia, *Int. Rev. Phys. Chem.*, 2006, **25**, 109–163.
20. D. B. Atkinson and M. A. Smith, *Rev. Sci. Instrum.*, 1995, **66**, 4434–4446.

21. T. Spangenberg, S. Kohler, B. Hansmann, U. Wachsmuth, B. Abel and M. A. Smith, *J. Phys. Chem. A*, 2004, **108**, 7527–7534.
22. S. Lee, R. J. Hoobler and S. R. Leone, *Rev. Sci. Instrum.*, 2000, **71**, 1816–1823.
23. S. E. Taylor, A. Goddard, M. A. Blitz, P. A. Cleary and D. E. Heard, *Phys. Chem. Chem. Phys.*, 2008, **10**, 422–437.
24. J. M. Oldham, C. Abeysekera, B. Joalland, L. N. Zack, K. Prozument, I. R. Sims, G. B. Park, R. W. Field and A. G. Suits, *J. Chem. Phys.*, 2014, **141**(7), 154202.
25. S. B. Morales, Thesis, University of Rennes 1, Rennes (France), 2009.
26. S. Cheikh Sid Ely, S. B. Morales, J. C. Guillemin, S. J. Klippenstein and I. R. Sims, *J. Phys. Chem. A*, 2013, **117**, 12155–12164.
27. E. Jimenez, B. Ballesteros, A. Canosa, T. M. Townsend, F. J. Maigler, V. Napal, B. R. Rowe and J. Albaladejo, *Rev. Sci. Instrum.*, 2015, **86**, 045108.
28. D. Chastaing, P. L. James, I. R. Sims and I. W. M. Smith, *Faraday Discuss.*, 1998, **109**, 165–181.
29. D. Chastaing, P. L. James, I. R. Sims and I. W. M. Smith, *Phys. Chem. Chem. Phys.*, 1999, **1**, 2247–2256.
30. J. Bourgalais, V. Roussel, M. Capron, A. Benidar, A. W. Jasper, S. J. Klippenstein, L. Biennier and S. D. Le Picard, *Phys. Rev. Lett.*, 2016, **116**(5), 113401.
31. H. Sabbah, L. Biennier, S. J. Klippenstein, I. R. Sims and B. R. Rowe, *J. Phys. Chem. Lett.*, 2010, **1**, 2962–2967.
32. W. J. Tango, J. K. Link and R. N. Zare, *J. Chem. Phys.*, 1968, **49**, 4264–4268.
33. R. N. Zare, in *Annual Review of Analytical Chemistry, Vol 5*, ed. R. G. Cooks and E. S. Yeung, 2012, vol. 5, pp. 1–14.
34. B. R. Rowe, G. Dupeyrat, J. B. Marquette and P. Gaucherel, *J. Chem. Phys.*, 1984, **80**, 4915–4921.
35. N. Daugey, P. Caubet, B. Retail, M. Costes, A. Bergeat and G. Dorthe, *Phys. Chem. Chem. Phys.*, 2005, **7**, 2921–2927.
36. D. Carty, A. Goddard, S. Köhler, I. R. Sims and I. W. M. Smith, *J. Phys. Chem. A*, 2006, **110**, 3101–3109.
37. M. J. Howard and I. W. M. Smith, *J. Chem. Soc., Faraday Trans. II*, 1981, **77**, 997–1008.
38. I. W. M. Smith and D. W. A. Stewart, *J. Chem. Soc., Faraday Trans.*, 1994, **90**, 3221–3227.
39. S. Viti, E. Roueff, T. W. Hartquist, G. P. des Forets and D. Williams, *Ast. Astrophys.hys*, 2001, **370**, 557–569.
40. B. Larsson, R. Liseau, L. Pagani, P. Bergman, P. Bernath, N. Biver, J. H. Black, R. S. Booth, V. Buat, J. Crovisier, C. L. Curry, M. Dahlgren, P. J. Encrenaz, E. Falgarone, P. A. Feldman, M. Fich, H. G. Floren, M. Fredrixon, U. Frisk, G. F. Gahm, M. Gerin, M. Hagstrom, J. Harju, T. Hasegawa, A. Hjalmarson, L. E. B. Johansson, K. Justtanont, A. Klotz, E. Kyrola, S. Kwok, A. Lecacheux, T. Liljestrom, E. J. Llewellyn, S. Lundin, G. Megie, G. F. Mitchell, D. Murtagh, L. H. Nordh,

L. A. Nyman, M. Olberg, A. O. H. Olofsson, G. Olofsson, H. Olofsson, G. Persson, R. Plume, H. Rickman, I. Ristorcelli, G. Rydbeck, A. A. Sandqvist, F. V. Scheele, G. Serra, S. Torchinsky, N. F. Tothill, K. Volk, T. Wiklind, C. D. Wilson, A. Winnberg and G. Witt, *Ast. Astrophys.hys*, 2007, **466**, 999-U158.

41. R. Liseau, P. F. Goldsmith, B. Larsson, L. Pagani, P. Bergman, J. Le Bourlot, T. A. Bell, A. O. Benz, E. A. Bergin, P. Bjerkeli, J. H. Black, S. Bruderer, P. Caselli, E. Caux, J. H. Chen, M. de Luca, P. Encrenaz, E. Falgarone, M. Gerin, J. R. Goicoechea, A. Hjalmarson, D. J. Hollenbach, K. Justtanont, M. J. Kaufman, F. Le Petit, D. Li, D. C. Lis, G. J. Melnick, Z. Nagy, A. O. H. Olofsson, G. Olofsson, E. Roueff, A. Sandqvist, R. L. Snell, F. F. S. van der Tak, E. F. van Dishoeck, C. Vastel, S. Viti and U. A. Yildiz, *Ast. Astrophys.hys*, 2012, **541**, A73.
42. U. A. Yildiz, K. Acharyya, P. F. Goldsmith, E. F. van Dishoeck, G. Melnick, R. Snell, R. Liseau, J.-H. Chen, L. Pagani, E. Bergin, P. Caselli, E. Herbst, L. E. Kristensen, R. Visser, D. C. Lis and M. Gerin, *Ast. Astrophys.hys*, 2013, **558**, A58.
43. M. M. Teixidor and A. J. C. Varandas, *J. Chem. Phys.*, 2015, **142**, 014309.
44. I. W. M. Smith, A. M. Sage, N. M. Donahue, E. Herbst and D. Quan, *Faraday Discuss.*, 2006, **133**, 137–156.
45. H. Sabbah, L. Biennier, I. R. Sims, Y. Georgievskii, S. J. Klippenstein and I. W. M. Smith, *Science*, 2007, **317**, 102–105.
46. R. J. Cvetanovic, *J. Phys. Chem. Ref. Data*, 1987, **16**, 261–326.
47. R. J. Shannon, M. A. Blitz, A. Goddard and D. E. Heard, *Nat. Chem.*, 2013, **5**, 745–749.
48. R. J. Shannon, R. L. Caravan, M. A. Blitz and D. E. Heard, *Phys. Chem. Chem. Phys.*, 2014, **16**, 3466–3478.
49. I. R. Sims, *Nat. Chem.*, 2013, **5**, 734–736.
50. E. Jimenez, M. Antinolo, B. Ballesteros, A. Canosa and J. Albaladejo, *Phys. Chem. Chem. Phys.*, 2016, **18**, 2183–2191.
51. X. M. Yang and D. H. Zhang, *Z. Phys. Chem.*, 2013, **227**, 1247–1265.
52. D. A. Neufeld, P. Sonnentrucker, T. G. Phillips, D. C. Lis, M. De Luca, J. R. Goicoechea, J. H. Black, M. Gerin, T. Bell, F. Boulanger, J. Cernicharo, A. Coutens, E. Dartois, M. Kazmierczak, P. Encrenaz, E. Falgarone, T. R. Geballe, T. Giesen, B. Godard, P. F. Goldsmith, C. Gry, H. Gupta, P. Hennebelle, E. Herbst, P. Hily-Blant, C. Joblin, R. Kolos, J. Krelowski, J. Martin-Pintado, K. M. Menten, R. Monje, B. Mookerjea, J. Pearson, M. Perault, C. Persson, R. Plume, M. Salez, S. Schlemmer, M. Schmidt, J. Stutzki, D. Teyssier, C. Vastel, S. Yu, P. Cais, E. Caux, R. Liseau, P. Morris and P. Planesas, *Ast. Astrophys.hys*, 2010, **518**(5), L108.
53. A. Persky and H. Kornweitz, *Int. J. Chem. Kinet.*, 1997, **29**, 67–71.
54. M. Tizniti, S. D. Le Picard, F. Lique, C. Berteloite, A. Canosa, M. H. Alexander and I. R. Sims, *Nat. Chem.*, 2014, **6**, 141–145.

55. C. Zhu, R. Krems, A. Dalgarno and N. Balakrishnan, *Astrophys. J.*, 2002, **577**, 795–797.
56. C. Zhu, R. Krems, A. Dalgarno and N. Balakrishnan, *Astrophys. J.*, 2009, **703**, 1176.
57. D. A. Neufeld, M. G. Wolfire and P. Schilke, *Astrophys. J.*, 2005, **628**, 260–274.
58. P. S. Stevens, W. H. Brune and J. G. Anderson, *J. Phys. Chem.*, 1989, **93**, 4068–4079.
59. V. Aquilanti, S. Cavalli, D. De Fazio, A. Volpi, A. Aguilar and J. M. Lucas, *Chem. Phys.*, 2005, **308**, 237–253.
60. V. Aquilanti, K. C. Mundim, S. Cavalli, D. De Fazio, A. Aguilar and J. M. Lucas, *Chem. Phys.*, 2012, **398**, 186–191.
61. L. Biennier, H. Sabbah, V. Chandrasekaran, S. J. Klippenstein, I. R. Sims and B. R. Rowe, *Astron. Astrophys.*, 2011, **532**, A40.
62. L. Biennier, H. Sabbah, S. J. Klippenstein, V. Chandrasekaran, I. R. Sims and B. R. Rowe, *EAS Pub. Ser.*, 2011, **46**, 191–199.
63. M. Tizniti, S. D. Le Picard, A. Canosa, I. R. Sims and I. W. M. Smith, *Phys. Chem. Chem. Phys.*, 2010, **12**, 12702–12710.
64. S. D. Le Picard, M. Tizniti, A. Canosa, I. R. Sims and I. W. M. Smith, *Science*, 2010, **328**, 1258–1262.
65. R. P. Wayne, *Chemistry of atmospheres*, Oxford University Press, 3rd edn, 2000.
66. M. J. Pilling, S. H. Robertson and P. W. Seakins, *J. Chem. Soc., Faraday Trans.*, 1995, **91**, 4179–4188.
67. D. Fulle and H. Hippler, *J. Chem. Phys.*, 1996, **105**, 5423–5430.
68. S. M. Kathmann, *Theor. Chem. Acc.*, 2006, **116**, 169–182.
69. R. Zhang, A. Khalizov, L. Wang, M. Hu and W. Xu, *Chem. Rev.*, 2012, **112**, 1957–2011.
70. J. Merikanto, E. Zapadinsky, A. Lauri and H. Vehkamaki, *Phys. Rev. Lett.*, 2007, **98**, 145702.
71. J. Diemand, R. Angelil, K. K. Tanaka and H. Tanaka, *J. Chem. Phys.*, 2013, **139**, 15, 074309.
72. S. Hamon, S. D. Le Picard, A. Canosa, B. R. Rowe and I. W. M. Smith, *J. Chem. Phys.*, 2000, **112**, 4506–4516.
73. N. J. B. Green, *Comprehensive Chemical Kinetics: Unimolecular Kinetics, Part 1. The Reaction Step*, Elsevier, Amsterdam, 2003.
74. S. M. Kathmann, G. K. Schenter and B. C. Garrett, *J. Chem. Phys.*, 2002, **116**, 5046–5057.
75. K. D. Tucker, M. L. Kutner and P. Thaddeus, *Astrophys. J.*, 1974, **193**, L115.
76. A. Coustenis, B. Bézard, D. Gautier, A. Marten and R. Samuelson, *Icarus*, 1991, **89**, 152–167.
77. H. Beuther, D. Semenov, T. Henning and H. Linz, *Astrophys. J., Lett.*, 2008, **675**, L33–L36.
78. E. Herbst, *Chem. Phys. Lett.*, 1994, **222**, 297–301.

79. J. Bouwman, M. Fournier, I. R. Sims, S. R. Leone and K. R. Wilson, *J. Phys. Chem. A*, 2013, **117**, 5093–5105.
80. S. Soorkia, A. J. Trevitt, T. M. Selby, D. L. Osborn, C. A. Taatjes, K. R. Wilson and S. R. Leone, *J. Phys. Chem. A*, 2010, **114**, 3340–3354.
81. J. Niedzielski, W. Makulski and J. Gawłowski, *J. Photochem.*, 1978, **9**, 519–528.
82. S. Soorkia, C.-L. Liu, J. D. Savee, S. J. Ferrell, S. R. Leone and K. R. Wilson, *Rev. Sci. Instrum.*, 2011, **82**, 124102.
83. G. G. Brown, B. C. Dian, K. O. Douglass, S. M. Geyer, S. T. Shipman and B. H. Pate, *Rev. Sci. Instrum.*, 2008, **79**, 053103.
84. B. H. Pate and F. C. De Lucia, *J. Mol. Spectrosc.*, 2012, **280**, 1–2.
85. B. C. Dian, G. G. Brown, K. O. Douglass and B. H. Pate, *Science*, 2008, **320**, 924–928.
86. J. L. Neill, B. J. Harris, A. L. Steber, K. O. Douglass, D. F. Plusquellic and B. H. Pate, *Optics Express*, 2013, **21**, 19743–19749.
87. C. Abeysekera, B. Joalland, N. Ariyasingha, L. N. Zack, I. R. Sims, R. W. Field and A. G. Suits, *J. Phys. Chem. Lett.*, 2015, **6**, 1599–1604.
88. J. A. Montgomery, M. J. Frisch, J. W. Ochterski and G. A. Petersson, *J. Chem. Phys.*, 1999, **110**, 2822–2827.
89. J. A. Montgomery, M. J. Frisch, J. W. Ochterski and G. A. Petersson, *J. Chem. Phys.*, 2000, **112**, 6532–6542.
90. N. Balucani, O. Asvany, L. C. L. Huang, Y. T. Lee, R. I. Kaiser, Y. Osamura and H. F. Bettinger, *Astrophys. J.*, 2000, **545**, 892–906.
91. N. Balucani, O. Asvany, R. I. Kaiser and Y. Osamura, *J. Phys. Chem. A*, 2002, **106**, 4301–4311.
92. P. L. James, I. R. Sims and I. W. M. Smith, *Chem. Phys. Lett.*, 1997, **272**, 412–418.
93. P. L. James, I. R. Sims and I. W. M. Smith, *Chem. Phys. Lett.*, 1997, **276**, 423–429.
94. C. Abeysekera, L. N. Zack, G. B. Park, B. Joalland, J. M. Oldham, K. Prozument, N. M. Ariyasingha, I. R. Sims, R. W. Field and A. G. Suits, *J. Chem. Phys.*, 2014, **141**, 214203.